Pharmacogn. Res., 2027; 19(1):405-425.
https://www.phcogres.com

Original Article

Modulation of KEAP1/NRF2-Regulated Anticancer Chemopreventive Signalling Pathways by Anacardic Acid in MCF7-ARE Human Breast Cancer Cells

Sangita Panda[1,2], Enketeswara Subudhi[1], Anand Bhaskar[2,3], Dishant Maniar[2,3], Vivek Basudkar[4], Aswathi Biju[5], Siddharth Modi[2], Dilip Mehta[2,3], Sujit Nair[2,3,*]

[1]Centre for Biotechnology, Siksha 'O' Anusandhan University (Deemed to be University), Bhubaneswar, Odisha, INDIA.
[2]Cellular and Molecular Biotechnology Division, Phytoveda Pvt. Ltd., Mumbai, Maharashtra, INDIA.
[3]Cellular and Molecular Biotechnology Division, Viridis Biopharma Pvt. Ltd., Mumbai, Maharashtra, INDIA.
[4]College of Pharmacy, Duquesne University, Pittsburgh, Pennsylvania, UNITED STATES.
[5]Saveetha Medical College and Hospital, SIMATS, Chennai, Tamil Nadu, INDIA.

ABSTRACT

Background: Breast cancer is the most diagnosed cancer worldwide, with an escalating burden over the past decades. Anacardic Acid (AA), a phenolic lipid extracted from cashew nutshell, displays diverse therapeutic properties including anti-tumor effects. However, the molecular mechanisms underlying the anticancer effects of AA have not been fully explored. **Objectives:** This study examined the potential anti-cancer effects of AA on MCF7-ARE breast cancer cells *in vitro* by evaluating cell survival, free radical scavenging ability, cell migration, and NRF2 activation. **Materials and Methods:** Western blot analysis was performed to investigate protein expression associated with various signaling pathways, such as cell cycle regulation, PI3K/AKT/mTOR, apoptosis, AP-1, NRF2, and NF-κB. Additionally, immunofluorescence techniques were utilized to examine the cellular localization of NRF-2 and p-NF-κB. **Results:** AA markedly reduced cell viability and migration capacity of MCF7-ARE cells. AA dose-dependently induced apoptosis *via* activation of Caspase-3,-6,-7, reduced Bcl-2, Bcl-xl expressions and elevated expressions of Bax and GSK-3β. AA upregulated the antioxidant response pathway *via* NRF2 and elevated expression of antioxidant enzymes SOD1, GST, NQO-1 and HO-1. AA downregulated proteins associated with the NF-κB pathway including iNOS, IkB/α and IL-2. AA treatment regulated the cell cycle progression pathway *via* downregulated BRCA1, HDAC, p-CDK2 expression and elevated p-eNOS and HIF1α expression. Immunofluorescence studies demonstrated that AA treatment triggered the migration of NRF2 from the cytoplasmic region to the nucleus, while concurrently diminishing the signal strength of p-NF-κB. **Conclusion:** Taken together, AA may be a promising chemopreventive agent against breast cancer progression.

Keywords: Anacardic Acid, Biomarkers, Breast Cancer, Cancer Chemoprevention, Cell Signaling.

Correspondence:
Dr. Sujit Nair
[1]Cellular and Molecular Biotechnology Division, Phytoveda Pvt. Ltd., Mumbai-400022, Maharashtra, INDIA.
[2]Cellular and Molecular Biotechnology Division, Viridis Biopharma Pvt. Ltd., Mumbai, Maharashtra, INDIA.
Email: sujit108@gmail.com
ORCID: 0000-0002-7322-7375

Received: 19-05-2026;
Revised: 08-07-2026;
Accepted: 27-08-2026.

INTRODUCTION

Breast cancer is the most common malignancy among women and remains a leading cause of cancer-related mortality. According to the GLOBOCAN report, female breast cancer accounts for approximately 11.6% of the 20 million new cancer cases worldwide and contributes to 6.9% of all cancer deaths, ranking second only to lung cancer. In India, breast cancer represents the most prevalent cancer type, followed by cancers of the lip and oral cavity, cervix uteri, lung, and esophagus (Bray *et al.*, 2024).

The global burden of breast cancer is projected to exceed 3 million new cases and 1 million deaths annually by 2040, largely driven by population growth and aging (Arnold *et al.*, 2022). Current treatment strategies include surgery, radiotherapy, and both neoadjuvant and adjuvant therapies (Burguin *et al.*, 2021). While these interventions have improved patient outcomes, there remains a persistent need to develop more effective and accessible therapeutic approaches for diverse patient populations.

In recent years, phytochemicals have gained significant attention for their potential in treating various diseases, including breast cancer. Anacardic Acid (AA), a phenolic lipid derived from the shell of the cashew nut (*Anacardium occidentale*), has been reported to exhibit a broad range of therapeutic activities such as antioxidant and anti-inflammatory effects (Gomes *et al.*, 2020), neuroprotective (Silva *et al.*, 2021), antibacterial (Hollands *et al.*, 2016), anticancer (Omanakuttan *et al.*, 2012), and antidiabetic

OPEN ACCESS

Manuscript TECHNOMEDIA

DOI: 10.5530/pres.20270159

properties (Tedong *et al.*, 2010). Several studies have demonstrated the anticancer potential of AA across various cancer types. Park *et al.* reported that AA enhances the efficacy of chemotherapy and suppresses pancreatic cancer growth by modulating the Chmp1A-ATM-p53 signaling pathway (Park *et al.*, 2018). Tan *et al.* observed that AA induces apoptosis in prostate cancer cells through inhibition of the ER stress/DAPK3/Akt pathway (Tan *et al.*, 2017). In MCF-7 breast cancer cells, AA hinders metastasis by blocking VEGF signaling, upregulating E-cadherin, and downregulating Twist and Snail, thereby preventing Epithelial-Mesenchymal Transition (EMT) (Shilpa *et al.*, 2015). Additionally, AA impedes breast cancer cell proliferation by interfering with the Oxidative Phosphorylation (OXPHOS) pathway (Radde *et al.*, 2016). It also induces cell death and G0/G1-phase arrest, effectively limiting the growth of MDA-MB-231 Triple-Negative Breast Cancer (TNBC) cells (Zhao *et al.*, 2018). Lucas *et al.* further demonstrated that AA modulates immune responses in breast cancer, particularly in TNBC, by regulating PD-L1 expression through NF-κB activation. This regulation promotes apoptosis via increased expression of γH2AX and cleaved caspase-3, thereby reducing tumor cell viability (Lucas *et al.*, 2018). Moreover, AA suppresses breast cancer progression by impairing lipid biosynthesis and inducing endoplasmic reticulum stress (Piell *et al.*, 2024). Previous studies have demonstrated the anticancer potential of AA (Muzaffar *et al.*, 2016); however, its specific effect on the NRF2/ARE signaling pathway in MCF7-ARE cells has not yet been investigated. The present study intended to elucidate the potential impact of AA in NRF2-reporter MCF7-ARE human breast cancer cells by integrating functional and molecular mechanisms and systematically examine the impact of AA's anti-proliferative and pro-apoptotic effects on cell viability, antioxidant capacity, and migration, together with its ability to modulate NRF2/ARE signaling and multiple oncogenic pathways, including PI3K/AKT/mTOR, NF-κB, AP-1, apoptosis, cell-cycle control, and hypoxia responses in MCF7-ARE cells. Through this comprehensive pathway-centric approach, the study sought to define whether AA can simultaneously activate cytoprotective antioxidant defences and suppress pro-survival signaling networks, thereby supporting its development as a promising chemopreventive candidate in breast cancer.

MATERIALS AND METHODS

Chemicals and reagents

The CellTiter 96® AQueous Non-Radioactive Cell Proliferation Assay Kit (G5421) procured from Promega (USA). Primary antibodies were acquired from Abcam (USA) and Cell Signaling Technology (USA); see Table S1 for more details. Firefly Luciferase Lysis Buffer 5× (LS-001) and Substrate (LUC100) were obtained from Signosis (USA). Ascorbic acid (purity 98%) was sourced from Sigma-Aldrich (USA).

Cell culture and cell viability

The NRF2/ARE luciferase reporter MCF7 stable cell line (MCF7-ARE) was obtained from Signosis, USA. Cells were routinely cultured in high-glucose DMEM (HiMedia, India) supplemented with 10% fetal bovine serum (HiMedia, India), penicillin (100 U/mL), and streptomycin (100 µg/mL). Cultures were maintained in a humidified incubator at 37±0.5°C with 5% CO_2 [Heracell, Thermo Scientific, USA]. For subculturing and plating, cells were first rinsed with Versene solution (0.1% EDTA in Dulbecco's phosphate-buffered saline; HiMedia, Cat# TCL020, India) to remove residual serum and chelate divalent cations. Cells were then dissociated using Trypsin-EDTA (HiMedia, India) and the reaction was neutralized with complete growth medium. Cell viability and density were assessed using the R^1 cell counter (Olympus, Japan) prior to seeding onto plates at desired densities or subculturing at a 1:3 to 1:5 ratio.

MTS assay

Cell viability was assessed using the CellTiter 96® AQueous Non-Radioactive Cell Proliferation Assay Kit (Promega, USA; G5421) based on the MTS (3-(4,5-dimethylthiazol-2-yl)-5-(3-carboxymethoxyphenyl)-2-(4-sulfophenyl)-2H-tetrazolium) assay. Cells (1×10^4 cells/well) were seeded into 96-well plates in triplicate. Based on preliminary results, AA concentrations ranging from 0 to 100 µM were selected. This concentration range was consistent with earlier studies (n=3). Experimental conditions were optimized to minimize variability, and appropriate controls were included to ensure accuracy and reproducibility. Following a 12-hr starvation period in medium containing 0.5% FBS, cells were incubated with the test compounds for 24, 48, and 72 hr at 37°C in a humidified incubator with 5% CO_2. After the incubation period, 20 µL of the MTS reagent was added to each well, and plates were further incubated for 3 hr at 37°C. Cell viability was determined by measuring absorbance at 490 nm using a Cytation 5 microplate reader (BioTek, USA).

Luciferase reporter assay

MCF7-ARE cells were plated in 96-well plates at a density of 1×10^4 cells per well and incubated for 24 hr at 37°C with 5% CO_2. Following a 12-hr serum starvation period in medium with 0.5% Fetal Bovine Serum (FBS), cells were treated with AA at concentrations ranging from 1 to 100 µM. Untreated cell controls were also included to validate the assay performance. Initial optimization experiments defined the optimal cell density, incubation time, and volumes of the reagents for consistent and reproducible results. After treatment, cells were further incubated for 24 hr at 37°C in a humidified atmosphere with 5% CO_2. For the luciferase assay, cells were washed once by discarding the culture medium and adding 100 µL Phosphate-Buffered Saline (PBS). Then, 20 µL of lysis buffer was added to each well and the plates were incubated at room temperature for 15 min. Finally, 50 µL of firefly luciferase substrate was added and the luminescence

measured immediately using a Cytation 5 microplate reader. The extent of NRF2 activation in the treated cells was calculated with regard to the controls. All experiments were conducted in triplicate to ensure statistical robustness.

Antioxidant activity

Antioxidant activity of AA in the MCF7-ARE cell line was determined using an EZAssay™ Antioxidant Activity Estimation Kit (CUPRAC, HiMedia, India) with minor modifications. MCF7-ARE cells were plated at a density of 2×10^7 in 6-well plates and incubated for 24 hr, followed by a starvation of 12 hr. In this experiment, cells were treated with AA at concentrations of 1, 5, and 10 µM for 24 hr. After the treatment, the culture medium was removed, and cells were washed with cold PBS before sonication on ice, which was done three times with a pulse duration of 10 sec on/off. Thereafter, 100 µL of deionized water was used to add 10 µL of the respective standards and samples to the wells. Finally, 100 µL of chromogenic substrate was added to the well and incubated at room temperature for 10 min. Absorbance was measured at 450 nm in a Cytation 5 microplate reader. Results were expressed as Trolox equivalents.

Cell migration assay

The migratory capability of MCF7-ARE cells was assessed by the scratch wound migration assay. Cells were seeded in 6-well plates at a density of 1×10^6 cells per well and maintained in complete medium until they reached ~80% confluency. After starvation with serum for 12 hr, the cells were incubated with AA at 0.5 and 10 µM for 36 hr. Using a sterile 200 µL pipette tip, a scratch was made through the cell monolayer. To remove floating cells, each well was washed three times with PBS; the adhering cells were then maintained in serum-free medium. Images of the scratched area were captured using an Olympus inverted microscope. Cell migration was quantified by measuring the cell-free gap area using ImageJ software at different time points. For each sample, images were analyzed in triplicate to measure the distance between the facing edges of the scratch. Scratch closure was calculated by comparing the width of the initial gap (time 0) to that at subsequent times using the formula:

$$\text{Cell migration rate (\%)} = \frac{(\text{Initial scratch area} - \text{Current scratch area})}{\text{Initial scratch area}} \times 100$$

Protein extraction

MCF7-ARE cells (2×10^5) were cultured in 6-well plates for 24 hr, followed by 12 hr of starvation in medium containing 0.5% FBS. Cells were treated with ascorbic acid at concentrations of 0.5, 2.5, 5, 7.5, 10, and 15 µM for 24 hr. Thereafter, the cells were washed three times with phosphate-buffered saline, ice-cold, and then proteins were extracted in RIPA buffer supplemented with protease inhibitors. The cells were lysed by sonication at 10-second on/off pulses while being kept on ice for 20 min. The lysates were centrifuged at 16,000 × g for 20 min at 4°C, after which the supernatant-containing total protein was collected. The protein concentration was measured using the BCA assay kit (ThermoFisher, USA; Cat. no. 23225) according to the manufacturer's instructions; the absorbance was measured at 540 nm using a multi-well plate reader.

Western blot analysis

To identify the proteins involved in breast cancer pathways, STRING analysis was performed (Figure S1). Based on the STRING cluster analysis, proteins involved in PI3K/AKT/mTOR, NRF2, and apoptosis pathways were identified and validated through Western blot analysis. MCF7-ARE cells were exposed to AA (0.5. 2.5, 5, 7.5,10 and 15 µM), and Western blot analysis was utilized to determine the expression of proteins involved in these pathways. 20 µg of protein from the untreated cell controls and AA-treated MCF-7-ARE cells were mixed with 1x Laemmli sample buffer and heated at 95°C for 5 min to denature the protein. The protein samples (20 µg each/lane) along with premixed molecular weight markers were subjected to electrophoresis using a Basic PowerPac system (Bio-Rad Laboratories, USA) on precast 10% SDS-polyacrylamide gels at 130 V for one h. Furthermore, proteins were transferred to a PVDF membrane employing the Trans-Blot Turbo method (Bio-Rad, USA). The membranes were blocked using 5% Bovine Serum Albumin (BSA) for 1 hr at room temperature. Following three washes using 1X TRIS-BUFFERED SALINE and 0.1% Tween® 20 detergent (TBST) (10 min/wash), blots were placed at 4°C overnight with the corresponding primary antibodies (Table S1) at (1:1000) dilutions whereas p-IkB/α (S32/36), p-PI3 Kinase p110α, p-PI3 Kinase p85, and Akt at dilutions of (1:800), and c-Fos, p-eNOS (Ser1177), p-Akt (Ser473), and IL2 at (1:750) dilutions. Preliminary optimization studies were conducted to determine suitable antibody concentrations, optimal exposure times, and signal specificity for Western blot analysis. After the primary antibodies were incubated, the membranes were exposed to anti-mouse and anti-rabbit secondary antibodies (diluted 1:5000) conjugated with Horseradish Peroxidase (HRP) for 1 hr at room temperature, and then cleansed three times with 1X TBST for 10 min each with gentle rocking. Protein expression was detected using the SuperSignal™ West Femto Maximum Sensitivity Substrate (ThermoFisher, USA). Images were captured by using Bio-Rad ChemiDoc™ MP System, and densitometry analysis of each band was conducted using the ImageJ software, with β-actin serving as the loading control. Protein expression levels were normalized with β-actin to account for loading variability and ensure accurate comparisons.

Immunofluorescence assay

The Nuclear translocation of phosphorylated NRF2 (p-NRF2) and intensity of p-NF-κB were measured with this immunocytochemical technique in accordance with the methodology outlined by Dutta *et al.* with slight modifications

(Dutta *et al.*, 2020). The cells were inoculated into six-well plates sealed with coverslips and grown for 24 hr at 37°C in a humidified incubator with 5% CO_2. Following 12 hr of starvation, the cells were subjected to 10 µM AA for 24 hr. Subsequently, the cells were fixed with ice-cold methanol with 0.3-0.5% Triton X-100 for membrane permeability, followed by blocking with 5% BSA. The cells were maintained at 4°C for the whole night with primary antibodies like anti-phospho-NRF2 and anti-phospho-NF-κB, at a dilution ratio of 1:200. Following a wash with 1x PBS buffer, the cells were incubated for 1 hr at room temperature with secondary antibodies (goat anti-rabbit FITC IgG, Alexa Fluor 488, or Alexa Fluor 555) diluted at 1:400. Further, cells were washed with 1x PBS and counterstained with DAPI to visualize the cell nuclei. Images were captured using a fluorescence microscope (Olympus, Japan) at 100x magnification. Colocalization and fluorescence intensity measurements were performed using ImageJ.

Image analysis and correlation assessment

To evaluate the colocalization of p-NRF2 and DAPI, two complementary analyses were performed using the ImageJ plugin. Images were analyzed as maximum-intensity projections to identify pixels with the highest intensity. After importing the images into Fiji, color channels were separated and distinguished. Correlation analysis was then conducted using Pearson's correlation coefficient and Manders' coefficients (M1 and M2) to validate the colocalization results. This dual-method approach ensured robust and reliable quantification of spatial overlap. Pearson's coefficient assesses the intensity-based correlation between two signals, with NRF2 (green) as Signal A and DAPI (blue) as Signal B, with a correlation range of -1 (no overlap) to +1 (perfect overlap). Manders' coefficients quantify the spatial overlap between two signals. The coefficient M1 indicates the proportion of the NRF2 signal that overlaps with the DAPI signal, while M2 represents the proportion of the DAPI signal that overlaps with NRF2. To ensure accurate measurements, background fluorescence is removed by adjusting threshold settings. These overlap values range from 0, signifying no overlap, to 1, indicating complete overlap. Thresholding is essential to eliminate background noise and achieve precise quantification of colocalization.

ImageJ was used to measure fluorescence intensity of blue and green signals. The process involved separating the channels through Image → Color → Split Channels. A Region of Interest (ROI) was then selected, and intensity quantification was performed using Analyze → Measure. Background fluorescence was corrected by subtracting intensity values measured from non-fluorescent areas, ensuring accurate fluorescence quantification. The Corrected Total Cell Fluorescence (CTCF) was calculated according to the following formula:

$$\text{Corrected total cell fluorescence (CTCF)} = \text{Integrated density} - (\text{Area of ROI} \times \text{Mean Background Fluorescence})$$

Statistical Analysis

All experiments were performed in triplicate at three biological time points. Results were expressed as mean±Standard Deviation (SD). Statistical analysis employed one-way ANOVA ($p<0.05$) and the unpaired, two-sample Student's *t-test* (immunofluorescence) to compare treated MCF7-ARE cells against the control group. GraphPad Prism 9 and Microsoft Excel were used for statistical evaluations.

RESULTS

AA activates the NRF2 signaling pathway in MCF7-ARE cells

To evaluate AA induced effect on NRF2 expression, luciferase assay was conducted using MCF7-ARE cells. The cells were

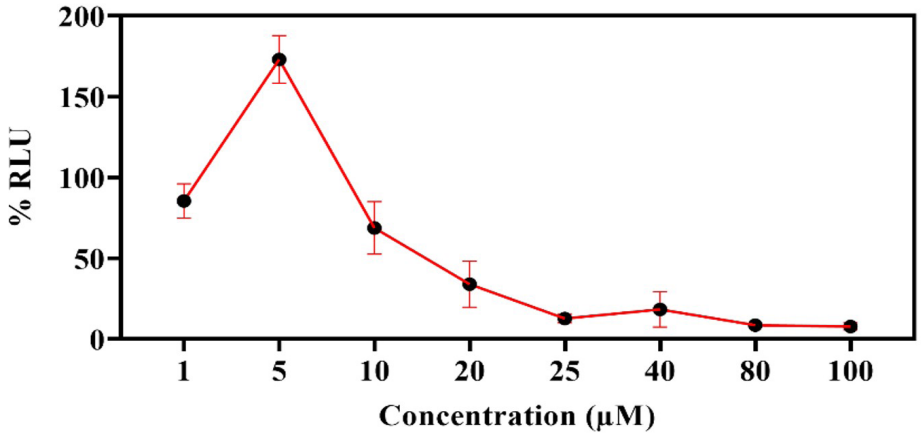

Figure 1: The effect of AA on NRF2 gene expression in MCF7-ARE cells using the luciferase assay.

subjected to AA at various doses (1-100 µM) for 24 hr. As shown in Figure 1, significant upregulation of NRF2 at a concentration of 5 µM AA was observed. NRF2 activation was increased by around 1.73-fold (RLU%=173.13±25.54) after treatment with 5 µM AA for 24 hr in comparison to the control group (Figure 1). Conversely, NRF2 activation decreased at higher AA concentrations possibly due to the cytotoxic effects at higher concentrations >10 µM. After 24 hr, no significant NRF2 activation was observed at lower concentrations *viz.* 0.5 µM and 1 µM. This result indicates a significant increase in NRF2 transcriptional activity, suggesting that AA effectively activates the NRF2 signaling pathway.

AA reduces cell viability in MCF7-ARE breast cancer cells in a dose-dependent manner

To identify the effect of AA on cell progression on MCF7-ARE cells, the MTS assay was conducted. As shown in Figure 2, AA treatment for 24 hr at concentrations of 0, 0.5,1, 2.5, 5, 10, 20, 25, 40, 80, and 100 µM resulted in cell viability of 100%, 58.11±4.69%, 67.40±4.37%, 66.14±2.80%, 64.06±3.26%, 67.66±5.55%, 50.86±2.94%, 31.75±6.59%, 12.75±6.43%, 7.53±5.88% and 3.96±0.90% respectively (Figure 2a); after 48 hr of AA treatment, cell viability was reduced to 100%, 53.63±5.98%, 56.16±3.27%, 54.85±1.56%, 50.91±4.15%, 56.08±9.74%, 22.25±3.60%, 7.84±1.47%, 7.53±2.5%, 3.17±3.17, 4.04±0.39%, respectively (Figure 2b); after 72 hr of AA treatment the cell viability was 100%, 52.66±2.53%, 58.54±1.64%, 59.22±2.64%, 57.83±5.83%, 40.52±7.37%, 17.14±0.15%, 10.64±2.77%, 11±5.95%, 9.47±3.47% and 6.8±3.79%, respectively (Figure 2c). Therefore, AA treatment significantly reduced the survival of MCF7-ARE in a dose-dependent manner with increasing concentration and longer exposure times resulting in greater reductions in MCF7-ARE cell survival. These findings suggest that AA effectively suppresses the progression of MCF7-ARE breast cancer cells, highlighting its potential as a therapeutic agent for targeting breast cancer.

AA enhances antioxidant capacity in MCF7-ARE cells

To determine the efficacy of the antioxidant activity of AA on MCF7-ARE cells, the Copper Reducing Antioxidant Capacity (CUPRAC) analysis was performed. Based on the cell viability analysis, 24 hr of exposure time was decided for subsequent experiments. The results of the CUPRAC assay demonstrated that AA significantly enhanced antioxidant capacity in MCF7-ARE cells in a dose-dependent manner. As shown in Figure 3, AA treatment at concentrations of 1, 5, and 10 µM increased antioxidant activity compared to the control group, with Trolox equivalent values rising progressively across doses. Statistical analysis indicated a minimal increase at 1 µM (not significant vs. control), a moderate increase at 5 µM (statistically significant), and a substantial increase at 10 µM (highly significant; ***$p<0.001$). These findings suggest that AA effectively augments the cellular antioxidant defense system in human breast cancer cells, as reflected by its elevated copper-reducing capacity.

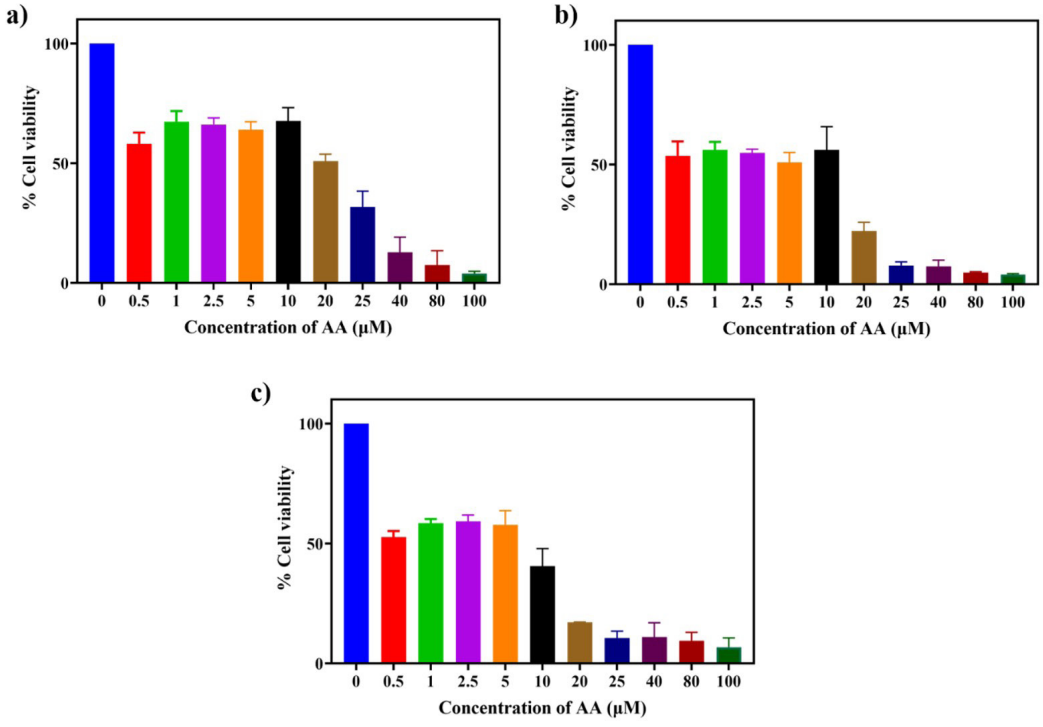

Figure 2: Effect of AA on MCF7-ARE cell viability over time and dose. AA suppresses the growth of MCF7-ARE human breast cancer cells. Cells were exposed to multiple concentrations of AA, namely 0, 0.5, 1, 2.5, 5, 10, 20, 25, 40, 80, and 100 µM, for durations of 24, 48, or 72 hr. Cell viability was evaluated by the MTS assay, and the results were expressed as the mean±Standard Error of Mean (SEM), with three replicates.

AA inhibits cell migration

Tumor cell migration is a vital component influencing the re-appearance and metastasis of breast cancer (Riaz *et al.*, 2024). To assess AA impact on cell migration, MCF7-ARE cells were subjected to two distinct concentrations of AA i.e., 0.5 µM and 10 µM for 36 hr. As shown in Figure 4, AA inhibited MCF7-ARE cell migration at both concentrations after 36 hr. The control group exhibited a significant 80% gap reduction which indicated migration of breast cancer cells. However, migration was significantly inhibited by AA at 0.5 µM and the gap was filled by around 50-60%, indicating a decrease in migration ability. Additionally, at 10 µM AA, the gap was not filled completely depicting a greater restriction on cell migration. The results are displayed as the mean value plus or minus the Standard Error of the Mean (SEM), (n=3), showing a significant difference of with (****p<0.0001) versus the control (Figure 4) AA displayed a suppressive effect on MCF7-ARE breast cancer cell migration, suggesting a possible therapeutic use for AA in cancer prevention.

AA modulates the PI3K/AKT/mTOR pathway

In human cancers, the PI3K/AKT/mTOR pathway is frequently upregulated because of the triggering of EGFR or Ras, along with mutations or loss in PI3K or AKT (Nambiar *et al.*, 2016). Treating MCF7-ARE cells with AA resulted in significant changes in the extent of protein expression related to the PI3K/AKT/mTOR signaling cascade at various doses. As shown in Figure 5, AA exhibits a dose-dependent remodeling of the PI3K/AKT/mTOR axis and several of its upstream and downstream regulators in MCF7-ARE cells, as evidenced by Western blot band intensities and corresponding densitometric bar graphs. At lower concentrations of AA, phosphorylation of central pro-survival components is already reduced, and this suppression becomes progressively stronger at higher doses, while multiple tumor-suppressive or stress-responsive proteins become increasingly activated. In the PI3K/AKT/mTOR core module, AA consistently diminished phosphorylated mTOR (Figures 5a, 5b), PI3K p110α (Figures 5a-5c), PI3K p85 (Figures 5a-5d), p-p70S6K (Figures 5a-5e) p-AKT at both Thr308 (Figures 5a-5f) and Ser473 (Figures 5a-5g) with the strongest inhibition observed between 10 and 15 µM. This pattern indicates that AA efficiently attenuates upstream PI3K activity, prevents full activation of AKT, and consequently reduces mTOR/p70S6K signaling, which is typically associated with cell growth, protein synthesis, and survival. The dose-dependent decline in these phosphorylated forms suggests that AA targets multiple nodes within the pathway rather than a single isolated component. Conversely, AA enhanced the phosphorylation of PTEN (Figures 6a, 6b), p53 (Figures 6a-6c), GSK-3β (Figures 6a-6d), and S6 (Ser 235/236) ribosomal protein (Figures 6a-6e) at higher concentrations (approximately 7.5-15 µM), as shown by both the increase in band intensity on the blots and the rising optical density values in the histograms. Elevation of p-PTEN and p-p53 supports activation of stress and damage-response programs, promoting cell-cycle arrest and apoptosis, while functioning as a counter-regulatory brake on PI3K/AKT signaling. Increased p-GSK3β (Figures 6a, 6d) and p-S6 ribosomal protein (Figures 6a, 6e) further reflect modulation of downstream growth and translational control checkpoints, consistent with a shift from a pro-survival to a growth-inhibitory environment under AA exposure. The results demonstrate that AA potentially modulates key proteins involved in the PI3K/AKT/mTOR pathway.

AA induces apoptosis in MCF7-ARE cells

AA has been reported to trigger apoptosis in mammalian cells by suppressing key survival and proliferative proteins (Harsha Raj *et al.*, 2016; Hollands *et al.*, 2016). Consistent with this, the present Western blot analysis showed that AA induced a marked, dose-dependent activation of apoptosis in MCF7-ARE cells. At lower doses (0.5-5 µM), AA caused minimal changes in apoptotic signaling; however, concentrations above 5 µM

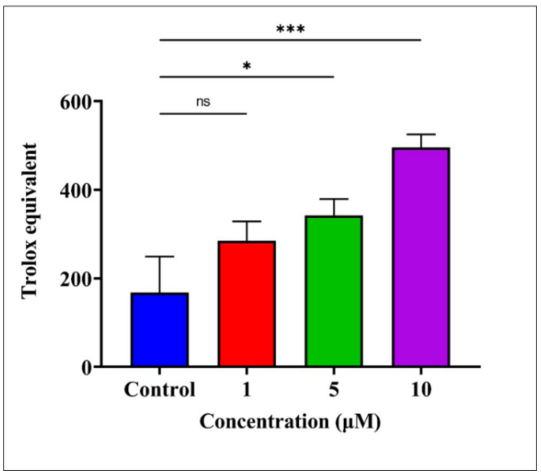

Figure 3: AA enhances antioxidant capacity in MCF7-ARE cells in a dose-dependent manner. Cells were treated with 1, 5, and 10 µM AA for 24 hr, and antioxidant activity was expressed as Trolox equivalents. Bar graph displays mean±SEM (n=3). Statistical analysis showed a significant increase in antioxidant capacity at 5 µM (*p<0.05) and a highly significant increase at 10 µM (***p<0.001) compared to the controls (untreated cells). ns - not significant.

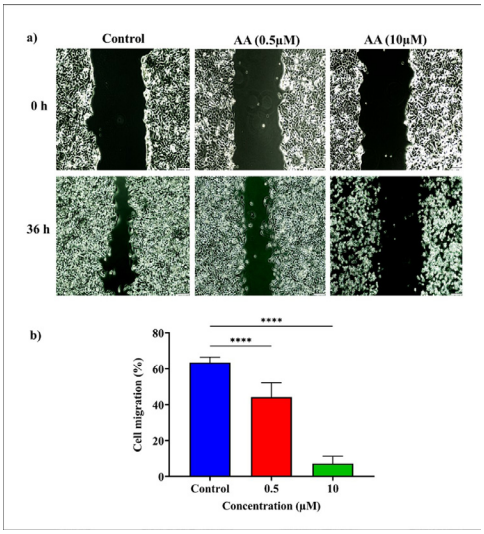

Figure 4: Inhibition of cell migration by AA. a) MCF7-ARE human breast cancer cells were treated with various concentrations of AA (0, 0.5, and 10 μM) for a duration of 36 hr to assess cellular migration capacity. b) Cells treated with 10 μM AA for 36 hr exhibited significantly reduced migration compared to untreated cells. Data are presented as mean±SEM (n=3), with ****p<0.0001 versus controls (untreated cells).

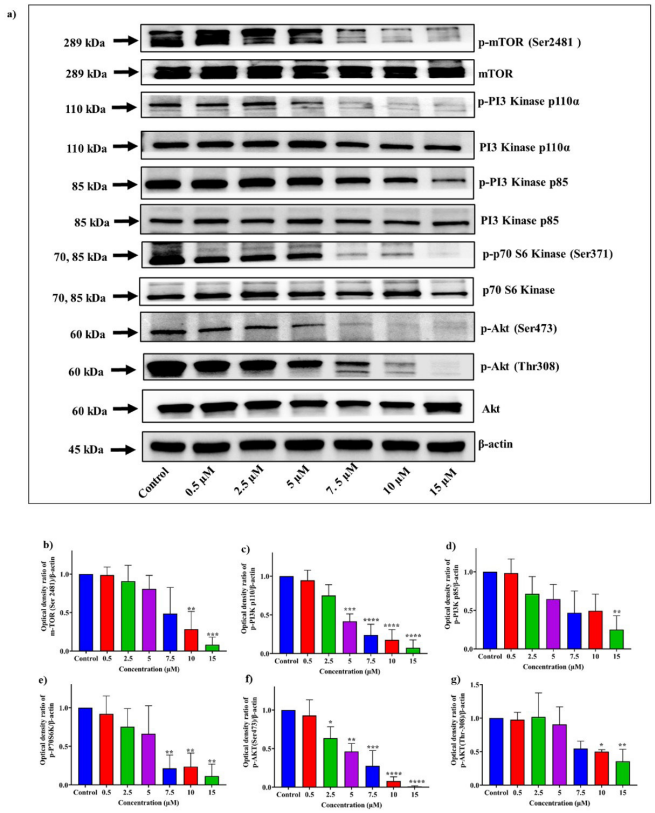

Figure 5: AA induces PI3K/AKT/mTOR Pathway regulation. a) Western blot images of p-mTOR, mTOR, p-PI3K110α, PI3K110α, p-PI3K85, PI3K85, p-p70S6K, p70S6K, p-Akt (Ser473), p-Akt (Thr308), AKT and -actin expression in cells treated with AA (0.5 to 15 μM). b - g) Densitometry of protein expression. Data are represented as mean±SEM (n=3). *p<0.03 **p<0.002, ***p<0.0002 and ****p<0.0001 versus controls (untreated cells).

produced pronounced alterations in the expression of multiple apoptosis-related proteins (Figures 7 and 8).

AA treatment led to a significant reduction in the anti-apoptotic proteins Bcl-xL, Bcl-2, and caspase-1,, , , which is associated with inflammatory cell death, thereby shifting the balance towards cell death signaling (Figures 7a-7d). In contrast, there was a robust elevation in the levels of pro-apoptotic caspases, including caspase-3, -6, -7, and -9, indicating efficient engagement of the caspase cascade and heightened breast cancer cell killing relative to untreated controls (Figures 8a-8d). In parallel, AA markedly increased the expression of the pro-apoptotic protein Bax in MCF7-ARE cells, supporting enhanced mitochondrial pathway activation (Figures 8a, 8e).

Furthermore, AA substantially upregulated the tumor suppressor p53 (Figures 6a, 6c), a central mediator of apoptosis in response to cellular stress and DNA damage, together with Bax, reinforcing the pro-apoptotic shift in MCF7-ARE cells (Figures 8a-8e). Densitometric analyses, presented as mean±SEM (n=3), confirmed these changes to be statistically significant, with *p<0.03, **p<0.002, ***p<0.0002, and ****p<0.0001 compared with control cells. Overall, these findings indicate that AA promotes apoptosis in MCF7-ARE cells primarily through activation of the caspase-dependent pathway and concurrent suppression of anti-apoptotic regulators.

AA activates NRF2/ARE signaling

NRF2/ARE signaling activation reduces oxidative damage, lessen inflammation and restore mitochondria, thereby enhancing the defense mechanism of the cells (Lin *et al.*, 2023). Oxidative stress is a factor in cancer, and NRF2 shields cells by triggering antioxidant and anti-inflammatory responses. In breast cancer, NRF2 activation can help stop the growth of tumors (Aliyev *et al.*, 2021). Treatment of MCF7-ARE cells containing various concentrations of AA for 24 hr resulted in significant modifications to the NRF2/ARE signaling pathway. Western blot and immunofluorescence assessments provided crucial insights into the stimulation of the NRF2 signaling cascade. Western blot results revealed that expression of phosphorylated NRF2 (p-NRF2) (Figures 9a, 9b) was elevated in a dose-dependent approach, particularly at higher concentrations *viz.* 7.5 µM, 10 µM, and 15 µM on contrary to the lower AA treatments. On the other hand, KEAP1, that normally inhibits NRF2 activation, was downregulated (Figures 9a, 9c) facilitated by substantial increase in p-NRF2 expression and nuclear translocation of NRF2. Simultaneously, Western blot analysis revealed the upregulation of key NRF2 target proteins such as GST (Figures 9a, 9d), NQO1 (Figures 9a, 9e), HO-1 (Figures 9a, 9f), and SOD1 (Figures 9a, 9g) at higher concentrations, further signifying an enhanced cellular antioxidant response to AA treatment by the MCF7-ARE cells.

AA stimulates NRF2 translocation

AA-mediated effects on NRF2 nuclear trafficking were evaluated in MCF7-ARE cells cultured on coverslips and exposed to 10 µM AA for 24 hr, followed by immunofluorescence analysis of p-NRF2 and DAPI staining. AA treatment produced a clear increase in nuclear green fluorescence compared with control cells, indicating enhanced activation and translocation of NRF2

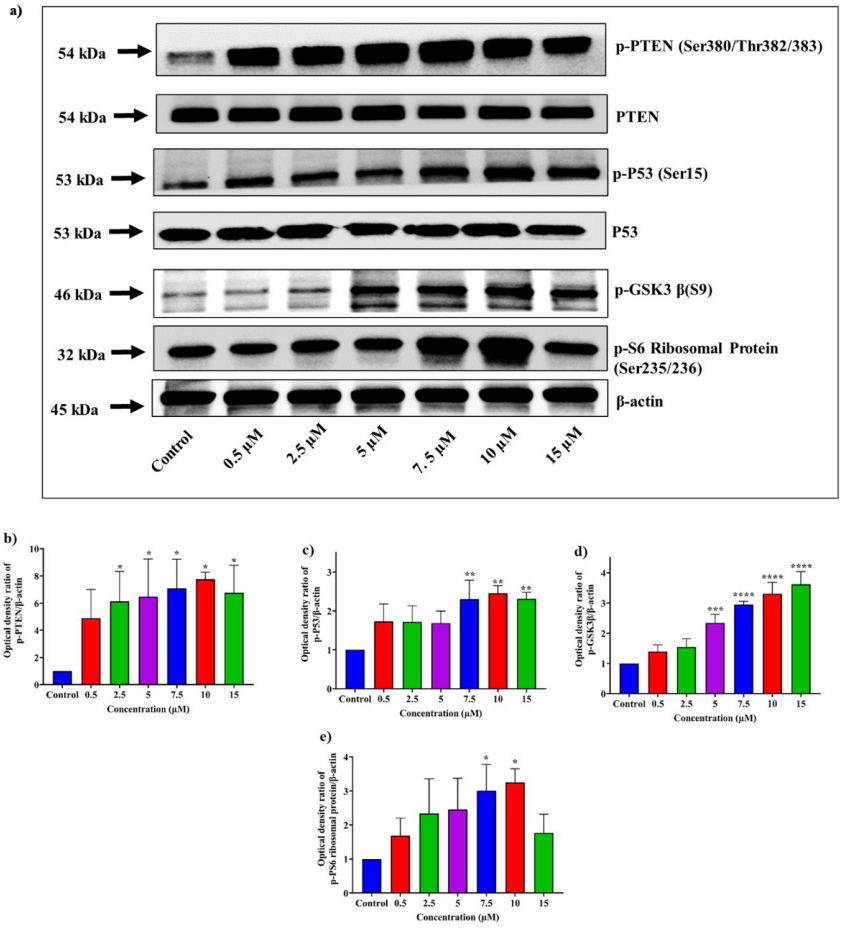

Figure 6: AA induces stress and damage responsive protein regulation. a) Western blot images of p-PTEN (Ser380/Thr382/383), PTEN, p-p53 (Ser15), P53, p-GSK3β, p-S6 ribosomal protein (Ser235/236) and -actin expression in cells treated with AA (0.5 to 15 µM). b-e) Densitometry of protein expression. Data are represented as mean±SEM (n=3). *p<0.03 **p<0.002, ***p<0.0002 and ****p<0.0001 versus controls (untreated cells).

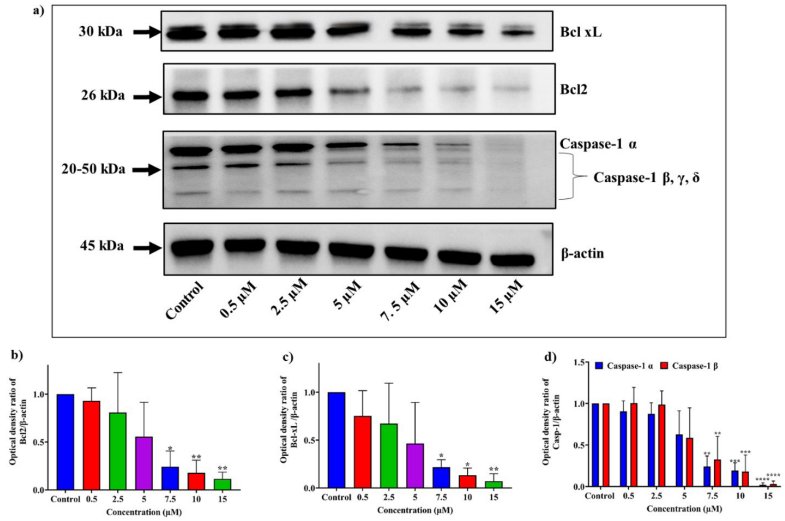

Figure 7: AA reduces anti-apoptotic protein regulation. a) Western blot images of BCL xL, BCL-2, caspase-1,, , . and -actin. b-d) Densitometry of protein expression. Data are represented as mean±SEM *(n=3). *p*< 0.03 ***p*< 0.002, ****p*< 0.0002 and *****p*< 0.0001 versus controls (untreated cells).

from the cytoplasm to the nucleus (Figure 10a). Quantitative colocalization analysis using Pearson's correlation coefficient demonstrated a significant rise in p-NRF2/DAPI overlap in AA-treated cells relative to controls. Control cells showed only moderate colocalization, with a mean coefficient of about 0.33 (range 0.166-0.611), whereas AA-treated cells exhibited a higher mean value of roughly 0.68 (range 0.305-1.0), confirming a statistically significant difference between groups (Figure 10b). To refine these observations, Manders' M1 and M2 coefficients were calculated using the Costes approach before and after thresholding. Without thresholding, no significant differences in M1 or M2 were detected between treated and control cells, suggesting that background signal partially masked true colocalization changes. Threshold application, which excluded nonspecific fluorescence, yielded control M1 values of 0.711-0.844 and M2 values of 0.669-0.999, while AA-treated cells displayed higher M1 values (0.833-1.0) and M2 values of 0.801-1.0. Costes threshold analysis further supported these findings: in controls, M1 ranged from 0.42 to 0.567 and M2 from 0.669 to 0.999, whereas AA-treated cells showed elevated M1 values (0.754-1.0) with M2 remaining between 0.801 and 0.999. These refined measurements confirmed a significant increase in M1, but not M2, indicating greater association of the p-NRF2 signal with DAPI-positive nuclei after AA exposure (Figures 10c, 10d). Together, the complementary colocalization metrics demonstrate that AA robustly promotes NRF2 nuclear accumulation and activation in MCF7-ARE cells, a change expected to potentiate antioxidant and cytoprotective gene expression programs. All data are presented as mean±SEM from three independent experiments, with differences considered significant at $p<0.05$.

AA modulates the NF-κB pathway

The NF-κB pathway orchestrates diverse physiological functions, including inflammation, innate and adaptive immunity, cell proliferation, haemostasis, and regulation of cell death (Zinatizadeh *et al.*, 2021). NF-κB is an essential transcription factor in cells that significantly contributes to the regulation of inflammation (Gazon *et al.*, 2018). Atypical or persistent stimulation of NF-κB plays a role in tumor development and resistance to treatment (Guo *et al.*, 2024). The translocation of the NF-κB p65 subunit to the nucleus is a crucial indicator of the activation of this pathway (Venugopal *et al.*, 2021). Western blot and immunofluorescence analyses were performed to clarify how AA influences this signaling axis in MCF7-ARE cells. At higher AA concentrations, a pronounced inhibition of NF-κB signaling was observed, indicating a concentration-dependent suppression of this pathway (Figures 11 and 12). Specifically, AA treatment markedly reduced the expression of inducible iNOS (Figures 11a, 11b), phosphorylated NF-κB p65 (Ser536) (Figures 11a, 11c), phosphorylated IκBα (S32/36) (Figure 11a, d), and IL-2 (Figures 11a, 11e), demonstrating attenuation of both upstream and downstream NF-κB components (Figure 11a). The decline in IL-2 confirmed reduced production of pro-inflammatory cytokines, supporting an anti-inflammatory effect of AA in this cellular context (Figures 11a, 11e). In parallel, downregulation of iNOS implied decreased nitric oxide synthesis, which is often associated with inflammatory and tumor-promoting signaling (Figures 11a, 11b). Collectively, these findings indicate that AA effectively suppresses NF-κB pathway activation in MCF7-ARE cells by downregulating key regulatory proteins and limiting pro-inflammatory mediator production.

Immunofluorescence data further revealed diminished p-NF-κB levels, consistent with reduced NF-κB activation and nuclear translocation, while decreased p-IκBα suggested impaired IκBα phosphorylation, thereby limiting NF-κB release from its inhibitor (Figure 12). Cells were grown for 24 hr and treated to 10 µM of AA to monitor NF-κB p65 activation within the cell nucleus. Results exhibited that cells treated with 10 µM AA

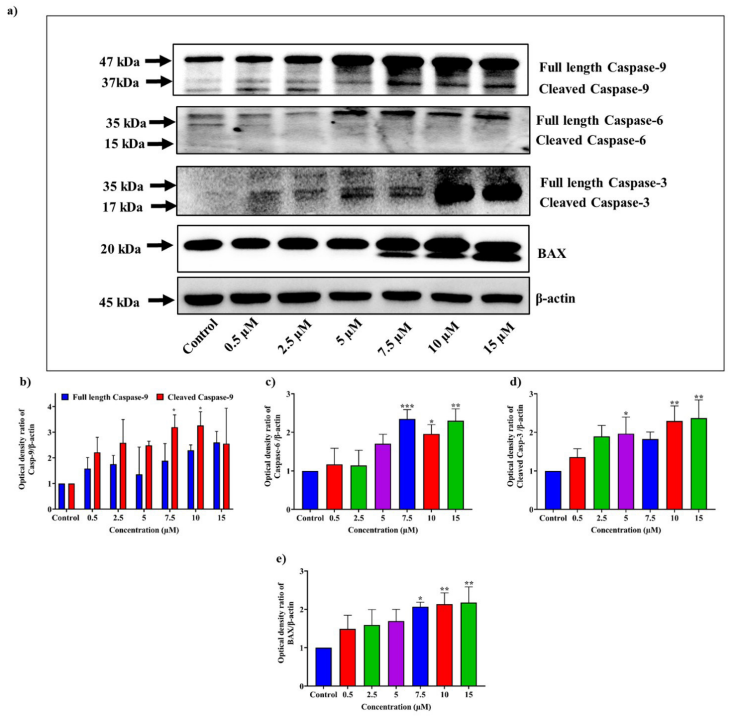

Figure 8: AA enhances the apoptosis pathway. a) Western blot images of caspase-9, caspase-6, caspase-3, Bax, and -actin. b-e) Densitometry of protein expression. Data are represented as mean±SEM (*n*=3). **p*<0.03 ***p*<0.002, ****p*<0.0002 and *****p*<0.0001 versus controls (untreated cells).

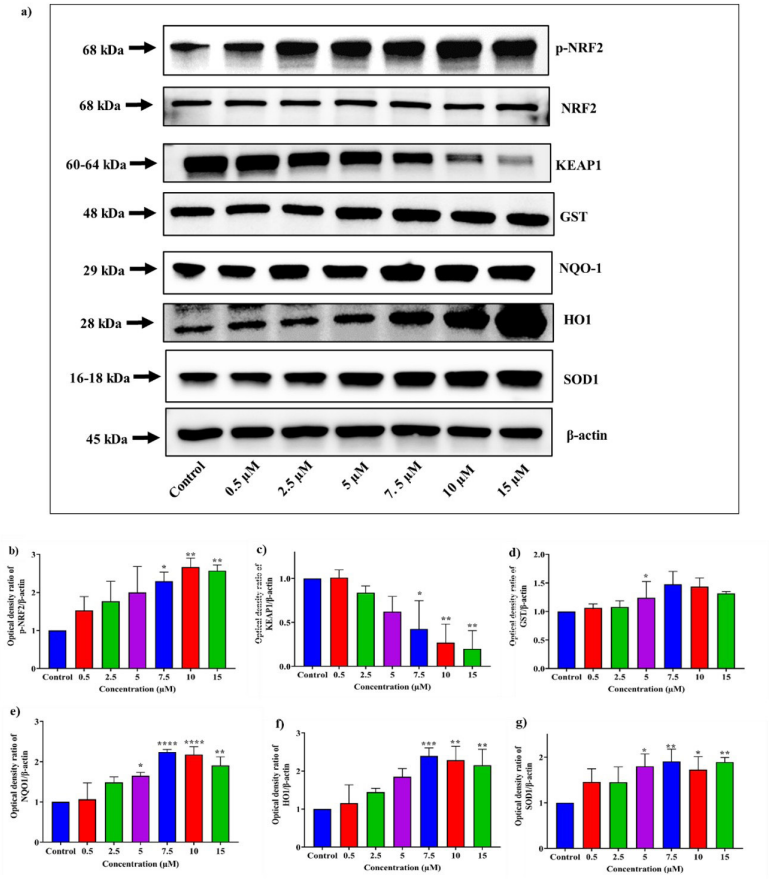

Figure 9: AA induces the antioxidant response pathway. a) Western blot analyses of p-NRF2, NRF2, KEAP-1, GST, NQO-1, HO1, SOD1 and -actin in MCF-ARE cells treated with AA (0.5-15 μM). b-g) Densitometry of protein expression. Data are represented as mean±SEM (*n*=3). **p*<0.03 ***p*<0.002, ****p*<0.0002 and *****p*<0.0001 versus controls (untreated cells).

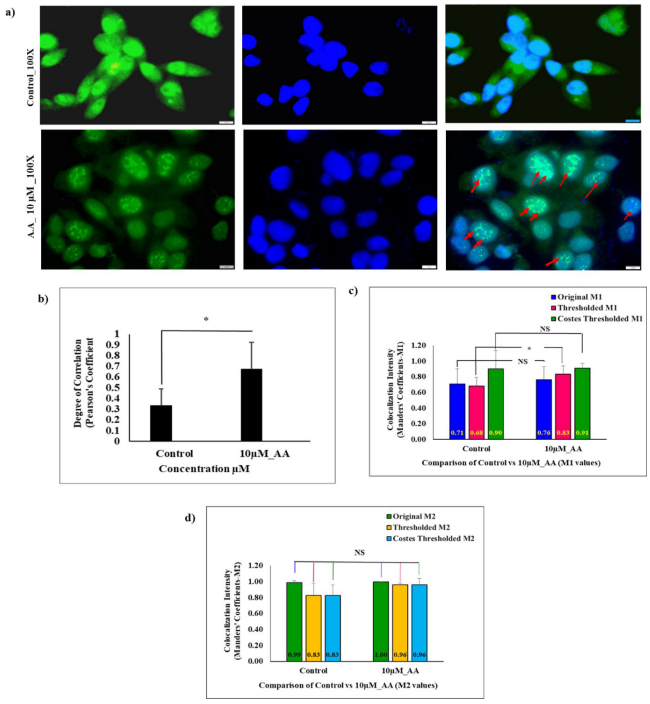

Figure 10: NRF2 localization in MCF7-ARE cells treated with 10 µM AA. Exposure of MCF7-ARE cells to 10 µM AA resulted in a significant change in the subcellular localization of NRF2. a) Immunofluorescence analysis showing NRF2 translocation from the cytoplasm to the nucleus (red arrow), evidenced by increased nuclear green fluorescence. b) Pearson's coefficient of co-localization. c) Manders' coefficient M1 (*p<0.05), and d) Manders' coefficient M2 (NS). Data presented as mean±SEM from three independent experiments. NS - Not Significant.

had significantly lowered the levels of p-NF-kB than untreated cells (Figure 12a). Additionally, the increased fluorescence intensity in the nuclear region suggested that p-NF-κB p65 was moved into the nucleus, suggesting the modulation of NF-κB signaling pathway by AA. Results exhibited that the Region of Interest (ROI) for intensity quantification demonstrated that AA effectively prevents the activation of p-NF-kB signaling. Significant differences (**p<0.01, and ***p<0.001) were observed across three independent studies (Figure 12b), highlighting the consistent inhibitory effect of AA on this signaling pathway.

AA alters the AP-1 and cell cycle progression pathways

The AP-1 transcriptional complex is a key regulator of inflammation, proliferation, differentiation, and apoptosis in mammalian cells (Gazon *et al.*, 2018). To define the effect of AA on this pathway, MCF7-ARE cells were exposed to increasing concentrations of AA for 24 hr, and the expression of AP-1-related proteins was examined. Western blot analysis showed marked, dose-dependent modulation of AP-1 components following AA treatment (Figures 13a-13d). Specifically, AA markedly reduced the abundance of c-Fos (Figure 13a, b) and AP-1 (Figures 13a, 13d) proteins at higher concentrations (7.5, 10, and 15 µM), while concomitantly increasing the level of phosphorylated c-Jun (Figures 13a, 13c), a key AP-1 subunit (Figures 13a-13d). These alterations in c-Fos, p-c-Jun, and overall AP-1 levels suggest that AA reprograms AP-1 signaling, with potential consequences for cellular survival, proliferation, and stress responsiveness in MCF7-ARE cells.

Moreover, AA treatment for 24 hr in MCF7-ARE cells exhibited notable changes in the expression of several crucial proteins involved in the development of the cell cycle regulation. AA treatment of MCF7-ARE cells resulted in the downregulation of several vital proteins involved in cell cycle regulation and DNA repair *viz.* BRCA1, Cyclin D1, p-CDK2, pRB, HDAC, NAT-10, and p-ACE2 indicating a major disruption of the cell cycle and a reduction in the growth of tumor cells (Figures 14a-14g). Simultaneously, AA elevated the production of critical hypoxia-related proteins like HIF-1α and p-eNOS, which are vital for cells to adapt to low oxygen (15a-d). Treatment of AA higher concentrations (7.5, 10, and 15 µM) resulted in substantial increase in hypoxia-related proteins demonstrated significantly stronger effects on MCF7-ARE cells in a dose-dependent manner. Our findings showed that AA has potent anticancer effect in MCF7 cancer cells by blocking the progression of the cell cycle and stimulating the hypoxia pathway (Figure 15).

DISCUSSION

Breast cancer is one of the most common cancers globally, with 2.3 million cases and 685,000 fatalities recorded in 2020 (Ombredane *et al.*, 2024). The overall number of cases exceeding 3 million by 2040 could lead to one million deaths each year attributed to age and population growth (Arnold *et al.*, 2022).

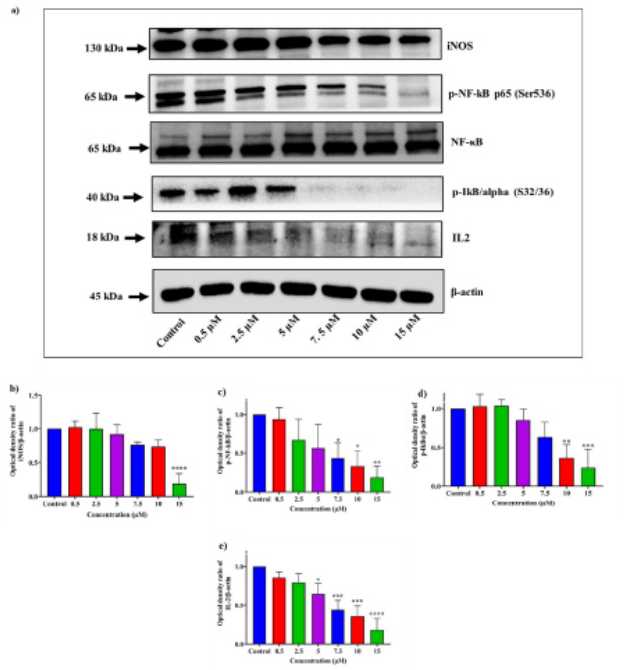

Figure 11: AA inhibits the NF-κB signaling pathway. a) Western blots of differentially expressed iNOS, p-NF-κB p65 (Ser536), NF-κB, p-IKB/ (S32/36), IL2 and -actin proteins on treatment with different AA concentrations (0.5-15μM). b-e) Densitometry of protein expression. Data are shown as mean±SEM for n=3 replicates, with statistically significant differences marked by *p< 0.03 **p< 0.002, ***p< 0.0002 and ****p< 0.0001 compared to controls.

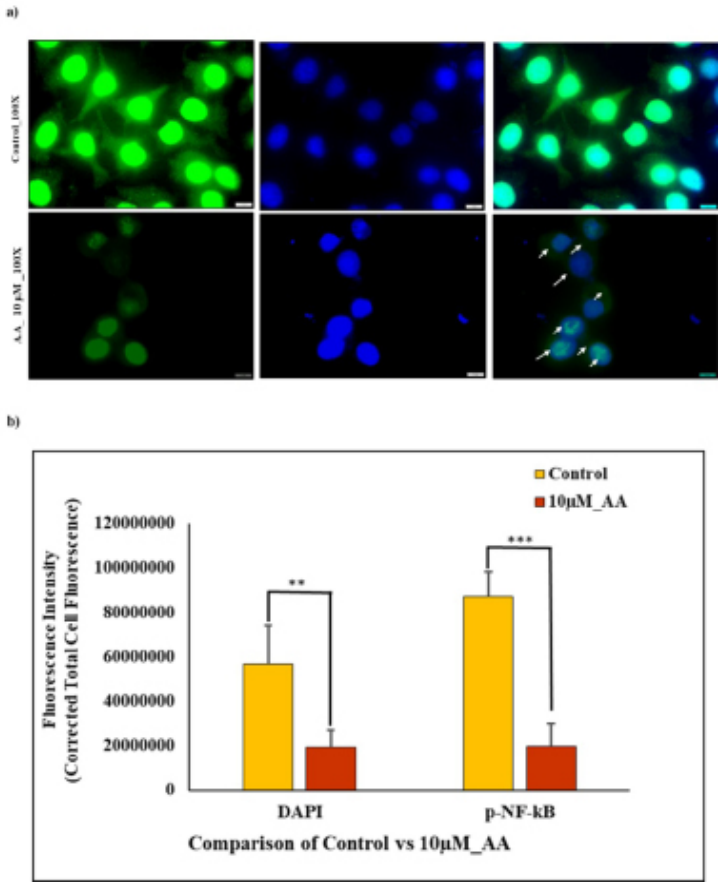

Figure 12: p-NF-κB localization in MCF7-ARE cells treated with 10 μM AA. The fluorescence intensities of proteins linked to the NF-κB signaling pathway in MCF7-ARE cells were significantly altered following treatment with 10 μM AA. (a) Immunofluorescence analysis showing decreased p-NF-κB levels in AA-treated cells compared to untreated controls, evidenced by decreased green fluorescence intensity (white arrow). (b) Corrected Total Cell Fluorescence (CTCF) comparison between AA-treated cells and untreated controls for DAPI and p-NF-κB. **p<0.01, and ***p<0.001. Data are presented as mean±SEM from n=3 independent experiments.

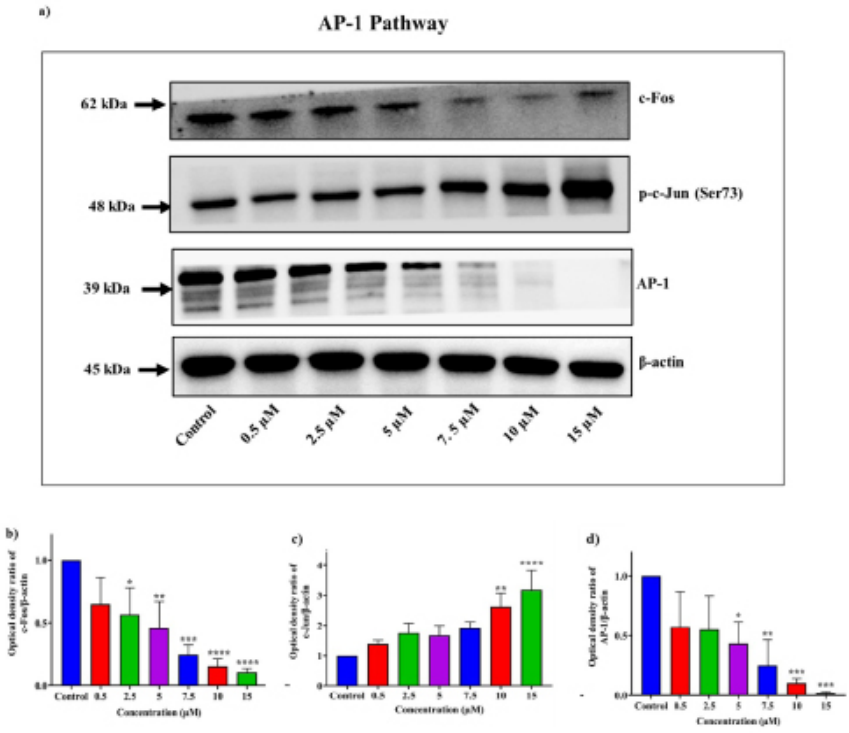

Figure 13: AA alters the AP-1 Pathway. a) Western blot images of differentially expressed proteins: c-Fos, c-Jun and AP-1 in MCF7-ARE cells on treatment with different concentrations of AA (0.5-15 µM). b-d) Densitometry of protein expression. Data are presented as mean±SEM (n=3), where *p<0.03 **p<0.002, ***p<0.0002 and ****p<0.0001 compared to controls.

AA, a bioactive constituent of *A. occidentale*, exhibits anticancer properties by hindering cell division and encouraging apoptosis. It holds anti-inflammatory, antibacterial, and antioxidant characteristics, reduces tumor growth (Radde *et al.*, 2016), and inhibits important enzymes such as NF-κB kinase, lipoxygenase, and histone acetyltransferases (Hemshekhar *et al.*, 2012; Ombredane *et al.*, 2024). The anti-proliferative effects of AA on different cancer cells have been extensively studied (Park *et al.*, 2018; Yao *et al.*, 2015; Zhao *et al.*, 2018). In cancer cells, the PI3K/AKT/mTOR pathway is crucial for regulating cell survival, proliferation, and metabolism (Glaviano *et al.*, 2023; Yang *et al.*, 2019). By obstructing this pathway, tumor growth is reduced by influencing key processes related to breast cancer development and progression, such as apoptosis, autophagy, and metastasis (Seyrek *et al.*, 2022). Malfunctioning AKT gain-of-function, PTEN loss, and PI3K hyperactivity are known factors contributing to cancer development and treatment resistance (Glaviano *et al.*, 2023). However, the specific mechanism in the MCF7-ARE breast cancer cell line remains unclear. In the present study, we described the effect of AA on MCF7-ARE cells at higher concentrations (>5 µM), where it was found to significantly reduce cell growth progression (Figure 2). The scratch assay indicated that cells exposed to 10 µM AA had lower migration rates than the control, supporting its anti-proliferative effects (Figure 4). AA induced apoptosis in MCF7-ARE cells by hindering the PI3K/AKT/mTOR pathway. Western blot analysis revealed that AA impacts the pathway by inhibiting its crucial proteins such as mTOR, PI3K p110, PI3K p85, p-P70S6K, and p-Akt (Thr308 and Ser473) which impedes cancer cell survival and metabolism. AA activates PTEN to inhibit the PI3K pathway, which served to restrict cell growth and increase p53 expression, promoting cancer cell death through apoptosis, and DNA repair (Figure 6). AA also triggers p-GSK3β and affects stress-induced protein synthesis through p-S6 ribosomal protein, enhancing the inhibition of cell division and apoptosis (Figure 6). Furthermore, our research indicates that AA induces apoptosis in MCF7-ARE cells by downregulating the anti-apoptotic proteins Bcl-2 and Bcl-xL, promoting mitochondrial membrane permeabilization, and reducing the expression of Caspase-1 (Figure 7). Additionally, elevated levels of Bax and caspase-3, -6, -7, and -9 confirm this apoptotic response, triggering the caspase cascade that leads to cell death (Figure 7). Our findings align with previous research demonstrating that AA causes apoptosis in various cancer types, including breast cancer (Gnanaprakasam *et al.*, 2021; Zhao *et al.*, 2018), prostate cancer (Tan *et al.*, 2017), hepatoma in HepG2 and myeloma in U266 cells (Huang *et al.*, 2014). Interestingly, AA modulates key apoptotic regulators and pathways, reinforcing its potential as an effective therapeutic agent for promoting cell death in cancer cells through apoptosis. This phenomenon can be explained by the dose- and temporal-dependent redox modulation by AA. Lower doses of AA induce antioxidant defenses via NRF2 activation, which may initially protect cells from oxidative damage (Figure 9). However, higher doses or prolonged exposure overwhelm these defenses, causing accumulative oxidative stress,

mitochondrial dysfunction, and activation of apoptotic cascades involving caspases and p53 (Figures 7, 8). AA treatment also markedly elevated the expression of p-NRF2, a critical indicator of the cellular antioxidant response, as well as GST, SOD1, HO1, and NQO1, which further supported an enhanced oxidative stress response (Figure 9). Normally, Keap1 acts as an inhibitor to promote the degradation of NRF2 (Lee and Hu, 2020). However, following AA treatment, we noticed a rise in the antioxidant protein p-NRF2 and a decrease in Keap1 expression. This indicates that AA disrupts the Keap1-NRF2 connection, enabling NRF2 to accumulate and initiate the antioxidant response. Using luciferase reporter, CUPRAC, and immunofluorescence assays, the findings further support that AA activates the NRF2/ARE pathway and triggers antioxidant responses, as indicated by the luciferase signal (Figure 1). The role of AA as both an antioxidant and a pro-oxidant in cancer cells may appear paradoxical but is context-dependent and not necessarily controversial. AA may increase antioxidant defenses by activating cellular pathways that enhance free radical scavenging, protecting normal and cancer cells from oxidative damage. Simultaneously, AA can promote the generation of Reactive Oxygen Species (ROS) to levels that trigger cancer cell apoptosis or inhibit tumor progression. This dual effect is common in many natural compounds, where low to moderate doses enhance antioxidant defenses, while higher doses or prolonged exposure induce oxidative stress beyond the cellular tolerance of cancer cells, leading to cell death. Thus, AA's modulation of ROS is a balance between protecting cells from oxidative damage and exploiting ROS-mediated cytotoxicity to eliminate cancer cells-not a direct contradiction but a nuanced therapeutic mechanism (Hollands *et al.*, 2016; Salehi *et al.*, 2020).

The CUPRAC assay similarly revealed a significant increase in antioxidant activity, suggesting improved cellular defenses (Figure 3). A study of the colocalization of p-NRF2 and DAPI in MCF7-ARE cells, carried out using fluorescence microscopy under both/and treatment conditions 10 µM AA provided significant findings on their interaction. We compared Pearson's correlation coefficients as reported by Costes, along with Manders'

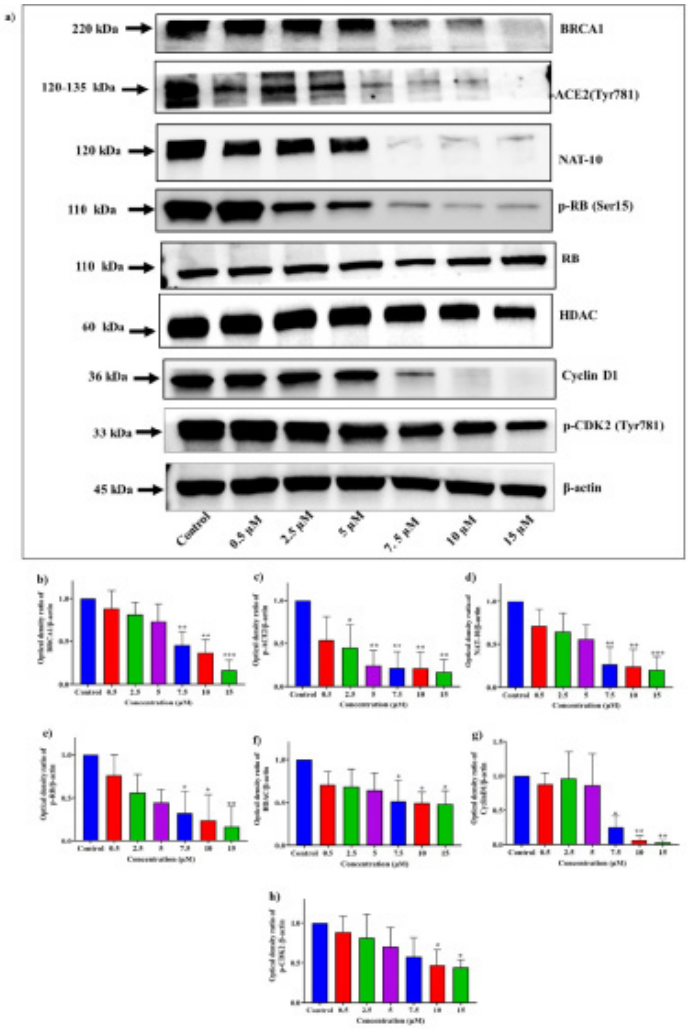

Figure 14: AA modulates the cell cycle regulation pathway. a) Western blot analysis of AA (0.5-15 µM) downregulating BRCA1, ACE2 (Tyr781), NAT10, p-Rb (Ser15), HDAC, cyclin D1 and p-CDK2 (Tyr781), while upregulating RB. b-h) Densitometry of protein expression. Data are presented as mean±SEM (n=3), with *p<0.03 **p<0.002, ***p<0.0002 and ****p<0.0001 versus controls.

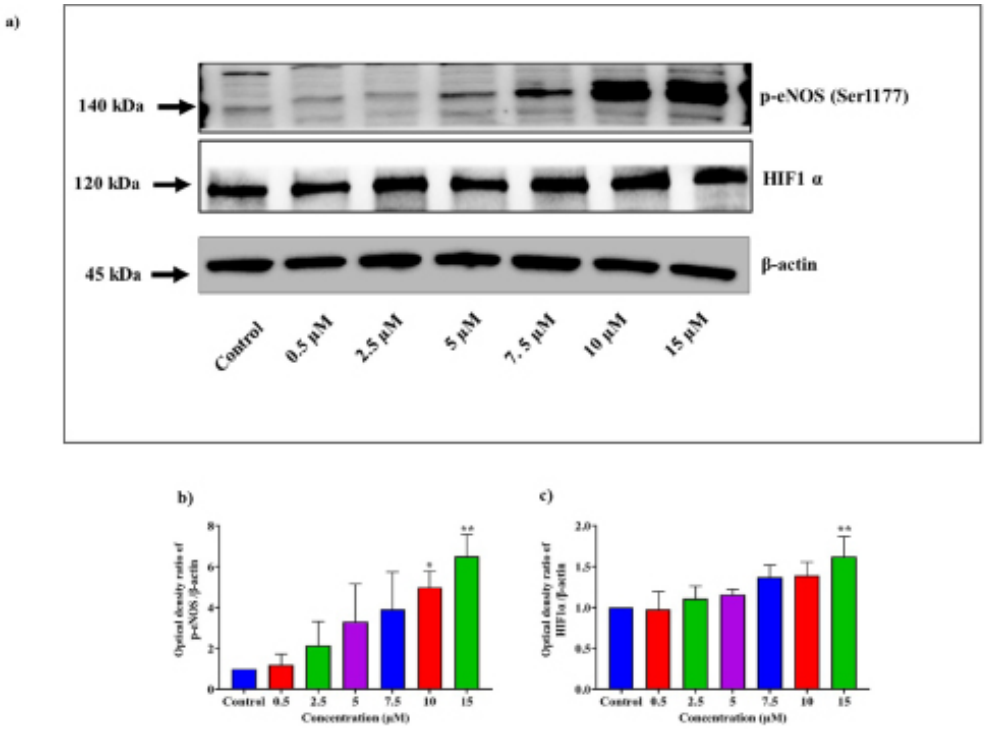

Figure 15: AA modulates the hypoxia pathway. a) Western blot analysis of AA (0.5-15 μM) upregulating p-eNOS (Ser1177) and HIF1. b,c) Densitometry of protein expression. Data are presented as mean±SEM (n=3), with *p<0.03 **p<0.002, ***p<0.0002 and ****p<0.0001 versus controls.

coefficients, to unravel the biological significance of these results under various conditions. Moreover, immunofluorescence analysis revealed a notable rise in nuclear p-NRF2 fluorescence intensity, validating that AA promotes NRF2 activation and nuclear translocation (Figure 12), which consequently enhances the antioxidant defenses within cells. Earlier studies indicating that AA, a histone acetyltransferase inhibitor, suppresses NF-κB-regulated protein products vital for cell survival and proliferation, enhances apoptosis, and reduces inflammation (Sung *et al.*, 2008). Further, AA's anti-inflammatory impact is amplified due to its reduction of IL-6 generation, nitric oxide production, and inflammatory marker expression (De *et al.*, 2018). Our Western blot results showed that AA suppressed the activation of NF-κB triggered by carcinogens, growth factors, and inflammatory agents. This was accomplished by decreasing the phosphorylation of IκBα at serine 32 and 36, which stopped its degradation, and reducing the phosphorylation of p65. Consequently, AA inhibited the NF-κB pathway, leading to a lessening of NF-κB regulated anti-apoptotic proteins (Bcl-2 and Bcl-xL) and iNOS expression. Moreover, the anti-inflammatory properties of AA were emphasized by lower levels of IL-2, a vital cytokine in controlling the immune system. Further supporting our findings, immunofluorescence experiments revealed a substantial reduction in p-NF-κB expression in cells treated with AA. This suggests that AA significantly reduces the NF-κB activation, as demonstrated by the nuclear translocation of p-NF-κB p65 and a decrease in p-NF-κB fluorescence intensity. AA treatment in MCF7-ARE cells markedly modulated the AP-1 signaling axis, with a pronounced reduction in AP-1 and c-Fos protein levels relative to control alongside an elevation in c-Jun expression. These coordinated changes in AP-1, c-Fos, and c-Jun imply that AA may function as an apoptosis inducer in breast cancer cells. Similarly, our research showed that AA treatment markedly inhibited critical proteins that play a role in cell cycle regulation, including NAT10, p-ACE2, BRCA1, p-Rb, HDAC, and p-CDK2, suggesting that it might disrupt the normal progression of the cell cycle and restrict cancer cell growth. Previous studies have shown that high Cyclin D1 levels promote the growth of both solid and hematologic tumors (Chen and Li, 2022). Moreover, our study exhibited that AA significantly reduced the expression of Cyclin D1, a crucial cell cycle regulator; however the absence of PTEN and p53 tumor suppressors causes cancer (Shin *et al.*, 2021). In contrast, AA treatment elevated the expression of p-eNOS and HIF1α, potentially activating HIF1α, a transcription factor crucial in low-oxygen environments, which may improve the cell's response to hypoxia.

Taken together, this study indicates that AA treatment lowers cell viability, causes cell cycle arrest, elevates apoptosis, inhibits significant signaling pathways including AP-1, NF-kB, PI3K/AKT/mTOR, and cell cycle regulation, and improves antioxidants in the MCF7-ARE breast cancer cell line. In addition, several important proteins, including caspase-1, -3, -9, Bcl-2, NRF2, AP-1, NF-kB, mTOR, AKT, PTEN, HIF1alpha, and p53, exhibit altered expression. Collectively, the findings suggest that AA may represent a promising strategy for preventing the development

of human breast cancers in the future. Further investigation is required to clarify these signaling pathways and optimize the therapeutic application of AA in cancer management.

CONCLUSION

In summary, our findings revealed the mechanistic basis for the promising anticancer chemopreventive effect of AA on MCF7-ARE breast cancer cells. AA significantly decreased oxidative stress by enhancing antioxidant activity, as demonstrated by the antioxidant capacity test. AA triggered the NRF2/ARE pathway, which upregulated the expression of antioxidant enzymes. AA suppressed cell migration in scratch assay experiments and regulated signaling pathways such as NF-κB, AP-1, NRF2, cell cycle regulation, PI3K/AKT/mTOR, and apoptosis. Overall, our results indicated that AA has putative potential in breast cancer treatment and targets multiple key pathways for suppressing cancer cell proliferation, migration, and survival. Future investigation is required to explore the potential and clinical significance of AA in breast cancer and other malignancies.

ABBREVIATIONS

AA: Anacardic acid; **MTS:** 3-(4,5-dimethylthiazol-2-yl)-5-(3-carboxymethoxyphenyl)-2-(4-sulfophenyl)-2H-tetrazolium; **FBS:** Fetal Bovine Serum; **HRP:** Horseradish peroxidase; **mTOR:** Mammalian target of rapamycin; **pAkt (T):** Phosphorylated AKT (Threonine); **pAkt (S):** Phosphorylated AKT (Serine); **pPI3Kα110:** Phosphorylated phosphoinositide 3-kinase alpha (110 kDa); **pPI3K85:** Phosphorylated phosphoinositide 3-kinase (85 kDa); **p-70S6K:** Phosphorylated 70 kDa S6 kinase; **AP1:** Activator protein 1; **Cyclin D1:** Cyclin D1; **Caspase-1:** Caspase-1; **BclXL:** B-cell lymphoma Extra Large; **KEAP-1:** Kelch-like ECH-associated protein 1; **IL2:** Interleukin 2; **E-cadherin:** Epithelial cadherin; **pNFκB:** Phosphorylated nuclear factor kappa-light-chain-enhancer of activated B cells; **cFos:** Cellular Fos; **Casp1:** Caspase-1; **pACE2:** Phosphorylated angiotensin-converting enzyme 2; **BRCA1:** Breast cancer 1; **NAT 10:** N-acetyltransferase 10; **pRB:** Phosphorylated retinoblastoma protein; **pNRF2:** Phosphorylated nuclear factor erythroid 2-related factor 2; **SOD1:** Superoxide dismutase 1; **HO-1:** Heme oxygenase 1; **NQO1:** NAD(P)H quinone dehydrogenase 1; **GSK3B:** Glycogen synthase kinase 3 beta; **Casp9:** Caspase-9; **Casp3:** Caspase-3; **Casp6:** Caspase-6; **Bax:** Bcl-2-associated X protein; **p53:** Tumor protein 53; **GST:** Glutathione S-transferase; **PTEN:** Phosphatase and tensin homolog; **GSK3 beta:** Glycogen synthase kinase 3 beta; **p-eNOS:** Phosphorylated endothelial nitric oxide synthase; **HIF1 alpha:** Hypoxia-inducible factor 1 alpha; **ROI:** Region of interest; **CTCF:** Corrected total cell fluorescence; **SD:** Standard deviation.

CONFLICT OF INTEREST

The authors declare that there is no conflict of interest.

FUNDING

This work was funded by Phytoveda Pvt. Ltd., Mumbai, India.

AUTHORS CONTRIBUTION

Sangita Panda: Investigation, Formal analysis, Software, Writing - original draft, Writing - review & editing, Visualization; **Enketeswara Subudhi:** Project administration; **Anand Bhaskar:** Writing - original draft, Writing - review and editing, Visualization; **Dishant Maniar:** Investigation, Formal analysis, Data curation; **Vivek Basudkar:** Investigation, Formal analysis, Data curation; **Aswathi Biju:** Formal analysis, Validation, Data curation; **Siddharth Modi:** Project administration; **Dilip Mehta:** Funding acquisition; **Sujit Nair:** Conceptualization, Supervision, Formal analysis, Writing - Review & editing, Project administration.

ETHICAL STATEMENT

This study utilized commercially available MCF7-ARE cell lines. No human participants or animal subjects were involved and therefore, specific ethical approval from an institutional review board was not required.

SUMMARY

This research shows that Anacardic Acid (AA) acts against the survival, proliferation and migration of MCF7-ARE breast cancer cells by reducing cell viability, arresting the cell cycle and inducing apoptosis. It also effected a reduction in oxidative stress by promoting antioxidant activity. This was effected by the regulation of the PI3K/AKT/mTOR, KEAP1/NRF2/ARE, NF-κB, and AP-1 pathways, along with several other major proteins, to exert an overall promising chemopreventive effect against breast cancer *in vitro*. Further research is required to investigate the specific mechanistic bases of protein regulation by anacardic acid and its clinical significance.

REFERENCES

Aliyev, A. T., Panieri, E., Stepani\' c, V., Gurer-Orhan, H., & Saso, L. (2021). Involvement of NRF2 in Breast Cancer and Possible Therapeutical Role of Polyphenols and Melatonin. Molecules, 26(7), 1853. https://doi.org/10.3390/molecules26071853

Arnold, M., Morgan, E., Rumgay, H., Mafra, A., Singh, D., *et al.* (2022). Current and future burden of breast cancer: Global statistics for 2020 and 2040. The Breast, 66, 15-23. https://doi.org/10.1016/j.breast.2022.08.010

Bray, F., Laversanne, M., Sung, H., Ferlay, J., Siegel, R. L., *et al.* (2024). Global cancer statistics 2022: GLOBOCAN estimates of incidence and mortality worldwide for 36 cancers in 185 countries. CA: A Cancer Journal for Clinicians, 74(3), 229-263. https://doi.org/10.3322/caac.21834

Burguin, A., Diorio, C., Durocher, F., Burguin, A., Diorio, C., *et al.* (2021). Breast Cancer Treatments: Updates and New Challenges. Journal of Personalized Medicine, 11(8), 808. https://doi.org/10.3390/jpm11080808

Chen, S., & Li, L. (2022). Degradation strategy of cyclin D1 in cancer cells and the potential clinical application. Frontiers in Oncology, 12, 949688. https://doi.org/10.3389/fonc.2022.949688

Da Silva, W. M. B., Pinheiro, S. de O., Alves, D. R., de Menezes, J. E. S. A., Magalhães, F. E. A., *et al.* (2021). Anacardic Acid Complexes as Possible Agents Against Alzheimer's Disease Through Their Antioxidant, *in vitro*, and *in silico* Anticholinesterase and Ansiolic Actions. Neurotoxicity Research, 39(2), 467-476. https://doi.org/10.1007/s12640-020-00306-w

De Souza, M. Q., Teotônio, I. M. S. N., de Almeida, F. C., Heyn, G. S., Alves, P. S., *et al.* (2018). Molecular evaluation of anti-inflammatory activity of phenolic lipid extracted from Cashew Nut Shell Liquid (CNSL). BMC Complementary and Alternative Medicine, 18(1), 181. https://doi.org/10.1186/s12906-018-2247-0

Dutta, S., Panda, S., Singh, P., Tawde, S., Mishra, M., *et al.* (2020). Hypopigmentation in burns is associated with alterations in the architecture of the skin and the dendricity of the melanocytes. Burns, 46(4), 906-917. https://doi.org/10.1016/j.burns.2019.10.003

Gazon, H., Barbeau, B., Mesnard, J.-M., & Peloponese, J.-M. (2018). Hijacking of the AP-1 Signaling Pathway during Development of ATL. Frontiers in Microbiology, 8, 2686. https://doi.org/10.3389/fmicb.2017.02686

Glaviano, A., Foo, A. S. C., Lam, H. Y., Yap, K. C. H., Jacot, W., *et al.* (2023). PI3K/AKT/mTOR signaling transduction pathway and targeted therapies in cancer. Molecular Cancer, 22(1), 138. https://doi.org/10.1186/s12943-023-01827-6

Gnanaprakasam, J. N. R., López-Bañuelos, L., & Vega, L. (2021). Anacardic 6-pentadecyl salicylic acid induces apoptosis in breast cancer tumor cells, immunostimulation in the host and decreases blood toxic effects of taxol in an animal model. Toxicology and Applied Pharmacology, 410, 115359. https://doi.org/10.1016/j.taap.2020.115359

Gomes Júnior, A. L., Islam, M. T., Nicolau, L. A. D., de Souza, L. K. M., Araújo, T. de S. L., *et al*.(2020). Anti-Inflammatory, Antinociceptive, and Antioxidant Properties of Anacardic Acid in Experimental Models. ACS Omega, 5(31), 19506-19515. https://doi.org/10.1021/acsomega.0c01775

Guo, Q., Jin, Y., Lin, M., Zeng, C., & Zhang, J. (2024). NF-κB signaling in therapy resistance of breast cancer: Mechanisms, approaches, and challenges. Life Sciences, 348, 122684. https://doi.org/10.1016/j.lfs.2024.122684

Harsha Raj, M., Yashaswini, B., R\" ossler, J., & Salimath, B. P. (2016). Combinatorial treatment with anacardic acid followed by TRAIL augments induction of apoptosis in TRAIL resistant cancer cells by the regulation of p53, MAPK and NFκβ pathways. Apoptosis: An International Journal on Programmed Cell Death, 21(5), 578-593. https://doi.org/10.1007/s10495-016-1223-8

Hemshekhar, M., Sebastin Santhosh, M., Kemparaju, K., & Girish, K. S. (2012). Emerging Roles of Anacardic Acid and Its Derivatives: A Pharmacological Overview. Basic & Clinical Pharmacology & Toxicology, 110(2), 122-132. https://doi.org/10.1111/j.1742-7843.2011.00833.x

Hollands, A., Corriden, R., Gysler, G., Dahesh, S., Olson, J., *et al.* (2016). Natural Product Anacardic Acid from Cashew Nut Shells Stimulates Neutrophil Extracellular Trap Production and Bactericidal Activity. Journal of Biological Chemistry, 291(27), 13964-13973. https://doi.org/10.1074/jbc.M115.695866

Huang, H., Hua, X., Liu, N., Li, X., Liu, S., *et al.* (2014). Anacardic acid induces cell apoptosis associated with induction of ATF4-dependent endoplasmic reticulum stress. Toxicology Letters, 228(3), 170-178. https://doi.org/10.1016/j.toxlet.2014.05.012

Lee, S., & Hu, L. (2020). Nrf2 activation through the inhibition of Keap1-Nrf2 protein-protein interaction. Medicinal Chemistry Research, 29(5), 846-867. https://doi.org/10.1007/s00044-020-02539-y

Lin, L., Wu, Q., Lu, F., Lei, J., Zhou, Y., *et al.* (2023). Nrf2 signaling pathway: Current status and potential therapeutic targetable role in human cancers. Frontiers in Oncology, 13, 1184079. https://doi.org/10.3389/fonc.2023.1184079

Lucas, J., Hsieh, T.-C., Halicka, H. D., Darzynkiewicz, Z., & Wu, J. M. (2018). Upregulation of PD-L1 expression by resveratrol and piceatannol in breast and colorectal cancer cells occurs via HDAC3/p300-mediated NF-κB signaling. International Journal of Oncology, 53(4), 1469-1480. https://doi.org/10.3892/ijo.2018.4512

Muzaffar, S., Bose, C., Banerji, A., Nair, B. G., & Chattoo, B. B. (2016). Anacardic acid induces apoptosis-like cell death in the rice blast fungus *Magnaporthe oryzae*. Applied Microbiology and Biotechnology, 100(1), 323-335. https://doi.org/10.1007/s00253-015-6915-4

Nambiar, J., Bose, C., Venugopal, M., Banerji, A., Patel, T. B., *et al.* (2016). Anacardic acid inhibits gelatinases through the regulation of Spry2, MMP-14, EMMPRIN and RECK. Experimental Cell Research, 349(1), 139-151. https://doi.org/10.1016/j.yexcr.2016.10.007

Omanakuttan, A., Nambiar, J., Harris, R. M., Bose, C., Pandurangan, N., *et al.* (2012). Anacardic Acid Inhibits the Catalytic Activity of Matrix Metalloproteinase-2 and Matrix Metalloproteinase-9. Molecular Pharmacology, 82(4), 614-622. https://doi.org/10.1124/mol.112.079020

Ombredane, A. S., Martins, N. alia O., de Souza, G. M. V., Araujo, V. H. S., Szlachetka, \' Isis O., *et al.* (2024). Combinatory Effect of Pequi Oil (*Caryocar brasiliense*)-Based Nanoemulsions Associated to Docetaxel and Anacardic Acid (*Anacardium occidentale*) in Triple-Negative Breast Cancer Cells *in vitro*. Pharmaceutics, 16(9), 1170. https://doi.org/10.3390/pharmaceutics16091170

Park, M., Upton, D., Blackmon, M., Dixon, V., Craver, S., *et al.* (2018). Anacardic acid inhibits pancreatic cancer cell growth, and potentiates chemotherapeutic effect by Chmp1A - ATM - p53 signaling pathway. BMC Complementary and Alternative Medicine, 18(1), 71. https://doi.org/10.1186/s12906-018-2139-3

Piell, K. M., Poulton, C. C., Stanley, C. G., Schultz, D. J., Klinge, C. M., *et al.* (2024). Integrated Metabolomics and Transcriptomics Analysis of Anacardic Acid Inhibition of Breast Cancer Cell Viability. International Journal of Molecular Sciences, 25(13), 7044. https://doi.org/10.3390/ijms25137044

Radde, B. N., Alizadeh-Rad, N., Price, S. M., Schultz, D. J., & Klinge, C. M. (2016). Anacardic Acid, Salicylic Acid, and Oleic Acid Differentially Alter Cellular Bioenergetic Function in Breast Cancer Cells. Journal of Cellular Biochemistry, 117(11), 2521-2532. https://doi.org/10.1002/jcb.25544

Riaz, F., Zhang, J., & Pan, F. (2024). Forces at play: Exploring factors affecting the cancer metastasis. Frontiers in Immunology, 15, 1274474. https://doi.org/10.3389/fimmu.2024.1274474

Salehi, B., Gültekin-Özgüven, M., Kirkin, C., Özçelik, B., Morais-Braga, M. F. B., *et al.* (2020). Antioxidant, Antimicrobial, and Anticancer Effects of Anacardium Plants: An Ethnopharmacological Perspective. Frontiers in Endocrinology, 11, 295. https://doi.org/10.3389/fendo.2020.00295

Seyrek, K., Wohlfromm, F., Espe, J., & Lavrik, I. N. (2022). The cross-talk of autophagy and apoptosis in breast carcinoma: Implications for novel therapies? Biochemical Journal, 479(14), 1581-1608. https://doi.org/10.1042/BCJ20210676

Shilpa, P., Kaveri, K., & Salimath, B. P. (2015). Anti-metastatic action of anacardic acid targets VEGF-induced signalling pathways in epithelial to mesenchymal transition. Drug Discoveries & Therapeutics, 9(1), 53-65. https://doi.org/10.5582/ddt.2014.01042

Shin, J. W., Kim, S.-H., & Yoon, J. Y. (2021). PTEN downregulation induces apoptosis and cell cycle arrest in uterine cervical cancer cells. Experimental and Therapeutic Medicine, 22(4), 1-7. https://doi.org/10.3892/etm.2021.10534

Sung, B., Pandey, M. K., Ahn, K. S., Yi, T., Chaturvedi, M. M., *et al*.(2008). Anacardic acid (6-nonadecyl salicylic acid), an inhibitor of histone acetyltransferase, suppresses expression of nuclear factor-κB-regulated gene products involved in cell survival, proliferation, invasion, and inflammation through inhibition of the inhibitory subunit of nuclear factor-κBα kinase, leading to potentiation of apoptosis. Blood, 111(10), 4880-4891. https://doi.org/10.1182/blood-2007-10-117994

Tan, J., Jiang, X., Yin, G., He, L., Liu, J., *et al.* (2017). Anacardic acid induces cell apoptosis of prostatic cancer through autophagy by ER stress/DAPK3/Akt signaling pathway. Oncology Reports, 38(3), 1373-1382. https://doi.org/10.3892/or.2017.5841

Tedong, L., Madiraju, P., Martineau, L. C., Vallerand, D., Arnason, J. T., *et al.* (2010). Hydro-ethanolic extract of cashew tree (*Anacardium occidentale*) nut and its principal compound, anacardic acid, stimulate glucose uptake in C2C12 muscle cells. Molecular Nutrition & Food Research, 54(12), 1753-1762. https://doi.org/10.1002/mnfr.201000045

Venugopal, M., Nambiar, J., & Nair, B. G. (2021). Anacardic acid-mediated regulation of osteoblast differentiation involves mitigation of inflammasome activation pathways. Molecular and Cellular Biochemistry, 476(2), 819-829. https://doi.org/10.1007/s11010-020-03947-9

Yang, J., Nie, J., Ma, X., Wei, Y., Peng, Y., & Wei, X. (2019). Targeting PI3K in cancer: Mechanisms and advances in clinical trials. Molecular Cancer, 18(1), 26. https://doi.org/10.1186/s12943-019-0954-x

Yao, K., Jiang, X., He, Ieye, Tang, Y., Yin, G., Zeng, Q., *et al.* (2015). Anacardic acid sensitizes prostate cancer cells to radiation therapy by regulating H2AX expression. International Journal of Clinical and Experimental Pathology, 8(12), 15926-15932.

Zhao, Q., Zhang, X., Cai, H., Zhang, P., Kong, D., Ge, X., Du, M., Liang, R., & Dong, W. (2018). Anticancer effects of plant derived Anacardic acid on human breast cancer MDA-MB-231 cells. American Journal of Translational Research, 10(8), 2424-2434.

Zinatizadeh, M. R., Schock, B., Chalbatani, G. M., Zarandi, P. K., Jalali, S. A., *et al.* (2021). The Nuclear Factor Kappa B (NF-kB) signaling in cancer development and immune diseases. Genes & Diseases, 8(3), 287-297. https://doi.org/10.1016/j.gendis.2020.06.005

Cite this article: Panda S, Subudhi E, Bhaskar A, Maniar D, Basudkar V, Biju A, *et al*. Modulation of KEAP1/NRF2-Regulated Anticancer Chemopreventive Signalling Pathways by Anacardic Acid in MCF7-ARE Human Breast Cancer Cells. Pharmacog Res. 2027;19(1):405-25.

Table S1: List of antibodies.

Sl. No.	Short Form	Full name	Source	Catalog Number	Make	Dilution
1.	AP-1	Activator Protein 1.	Rabbit	A5968	SIGMA	1:2000
2.	Bcl-2 (124)	Bcl-2 (124)	Mouse	15071S	Cell Signaling (CS)	1:800
3.	Bax	Bcl-2-associated X protein	Rabbit	2774S	Cell Signaling (CS)	1:1000
4.	Bcl-xl	Bcl-xl	Rabbit	2762S	Cell Signaling (CS)	1:1000
5.	β-actin	Beta-actin	Rabbit	4967	Cell Signaling (CS)	1:1000
6.	BRCA1	Breast cancer type 1 susceptibility protein	Rabbit	9010S	Cell Signaling (CS)	1:1000
7.	Caspase-1	Caspase-1	Rabbit	2225T	Cell Signaling (CS)	1:1000
8.	Caspase-3	Caspase-3	Rabbit	9662S	Cell Signaling (CS)	1:1000
9.	Caspase-6	Caspase-6	Rabbit	9762T	Cell Signaling (CS)	1:1000
10.	Caspase-9	Caspase-9	Rabbit	9502S	Cell Signaling (CS)	1:1000
11.	c-Fos	c-Fos	Rabbit	4384S	Cell Signaling (CS)	1:1000
12.	c-Jun	c-Jun	Rabbit	AB40766	Abcam	1:1000
13.	Cyclin D1	Cyclin D1	Rabbit	2922S	Cell Signaling (CS)	1:1000
14.	HO-1	Heme oxygenase-1	Rabbit	70081S	Cell Signaling (CS)	1:1000
15.	HDAC1	Histone deacetylase 1	Rabbit	2062S	Cell Signaling (CS)	1:1000
16.	HIF1α	Hypoxia-inducible factor 1 alpha	Rabbit	18338	Cell Signaling (CS)	1:800

Sl. No.	Short Form	Full name	Source	Catalog Number	Make	Dilution
17.	iNOS	Inducible Nitric Oxide Synthase	Rabbit	13120S	Cell Signaling (CS)	1:1000
18.	IL-2	Interleukin 2	Rabbit	12239S	Cell Signaling (CS)	1:750
19.	KEAP1	Kelch-like ECH-associated protein 1	Rabbit	8047	Cell Signaling (CS)	1:1000
20.	NAT10	N-acetyltransferase 10	Rabbit	66548S	Cell Signaling (CS)	1:1000
21.	NQO1	NAD(P)H dehydrogenase, quinone 1	Mouse	3187S	Cell Signaling (CS)	1:1000
22.	NRF2	Nuclear factor erythroid 2–related factor 2	Rabbit	12721S	Cell Signaling (CS)	1:1000
23.	NF-κB p65	Nuclear factor kappa B p65	Rabbit	8242S	Cell Signaling (CS)	1:1000
24.	PI3K p85	Phosphoinositide 3-kinase p85	Rabbit	4292S	Cell Signaling (CS)	1:1000
25.	p-Akt (Ser473)	Phosphorylated Akt (Ser473)	Rabbit	9271S	Cell Signaling (CS)	1:750
26.	p-ACE2 (Y781)	Phosphorylated angiotensin-converting enzyme 2 (Tyr781)	Rabbit	67041S	Cell Signaling (CS)	1:750
27.	p-CDK2 (Thr160)	Phosphorylated cyclin-dependent kinase 2 (Thr160)	Rabbit	2561	Cell Signaling (CS)	1:1000
28.	p-eNOS (Ser1177)	Phosphorylated endothelial nitric oxide synthase (Ser1177)	Rabbit	9571	Cell Signaling (CS)	1:750
29.	p-GSK3 Beta (S9)	Phosphorylated glycogen synthase kinase 3 beta (Ser9)	Rabbit	AB75814	Abcam	1:1000
30.	p-IkB/Alpha	Phosphorylated inhibitor of kappa B alpha (S32/36)	Mouse	9246S	Cell Signaling (CS)	1:750
31.	p-mTOR (Ser2481)	Phosphorylated mechanistic target of rapamycin (Ser2481)	Rabbit	2974S	Cell Signaling (CS)	1:1000
32.	p-NF-κB p65 (Ser536)	Phosphorylated nuclear factor kappa B p65 (Ser536)	Rabbit	3033L	Cell Signaling (CS)	1:1000

Sl. No.	Short Form	Full name	Source	Catalog Number	Make	Dilution
33.	p-p53 (Ser15)	Phosphorylated p53 (Ser15)	Rabbit	9284S	Cell Signaling (CS)	1:1000
34.	p-p70 S6K (Ser371)	Phosphorylated p70 S6 kinase (Ser371)	Rabbit	9208S	Cell Signaling (CS)	1:1000
35.	p-PI3K p110 Alpha	Phosphorylated phosphoinositide 3-kinase p110 Alpha	Rabbit	BS-6417R	SIGMA	1:800
36.	p-PI3K p85/p55	Phosphorylated phosphoinositide 3-kinase p85 (Tyr458)/p55 (Y199)	Rabbit	4228S	Cell Signaling (CS)	1:800
37.	p-PTEN (Ser380/ Thr382/383)	Phosphorylated PTEN (Ser380/ Thr382/Thr383)	Rabbit	9554S	Cell Signaling (CS)	1:1000
38.	P-Rb (Ser780)	Phosphorylated retinoblastoma protein (Ser780)	Rabbit	9307S	Cell Signaling (CS)	1:1000
39.	p-S6 Ribosomal Protein	Phosphorylated S6 ribosomal protein (Ser235/236)	Rabbit	2211S	Cell Signaling (CS)	1:1000
40.	SOD1	Superoxide dismutase 1	Rabbit	37385S	Cell Signaling (CS)	1:1000
41.	T-Akt	Total Akt	Rabbit	9272S	Cell Signaling (CS)	1:1000
42.	T-mTOR	Total mechanistic target of rapamycin	Rabbit	2972S	Cell Signaling (CS)	1:1000
43.	T-p53 (7F5)	Total p53 (7F5)	Rabbit	2527S	Cell Signaling (CS)	1:1000
44.	T-p70 S6K	Total p70 S6 kinase	Rabbit	9202S	Cell Signaling (CS)	1:1000
45.	T-PI3K p110 Alpha	Total phosphoinositide 3-kinase p110 Alpha	Rabbit	4255S	Cell Signaling (CS)	1:1000
46.	T-pTEN	Total PTEN	Rabbit	9552S	Cell Signaling (CS)	1:1000
47.	T-Rb (D20)	Total retinoblastoma protein	Rabbit	9313S	Cell Signaling (CS)	1:1000
48.	T-S6 Ribosomal Protein	Total S6 ribosomal protein	Rabbit	2217S	Cell Signaling (CS)	1:1000

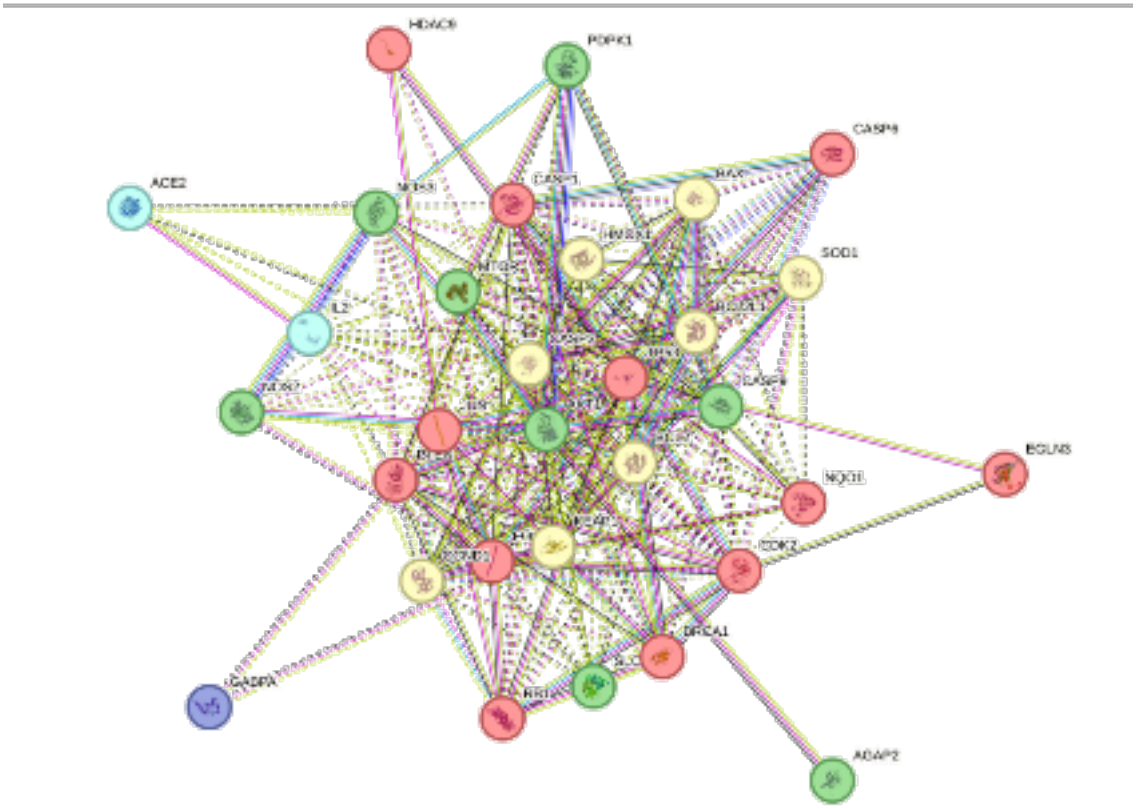

color	cluster Id	gene count	description
	Cluster 1	12	+ TP53 Regulates Transcription of Caspase Activators and Caspases
	Cluster 2	8	+ Epithelial cell apoptotic process
	Cluster 3	8	Constitutive Signaling by AKT1 E17K in Cancer
	Cluster 4	2	ACE2, IL2
	Cluster 5	1	GABPA

Figure S1: STRING analysis of proteins involved in breast cancer.